An examination of convective moistening of stratosphere

Ying Sun

Master of Science

Atmospheric and Oceanic Sciences

McGill University

Montreal, Quebec

2015-05-12

A thesis submitted to McGill University in partial fulfillment of the requirements of the degree of Master of Science

ACKNOWLEGEMENTS

Firstly I would like to express my gratitude to my great supervisor Yi Huang for the enlightening discussions, useful instructions and full support throughout this project. Thanks for the opportunities he gave me to present my work outside campus and learn to be a real scientist. I would also like to thank my student colleages and faculty, especially friends in my group who helped a lot with coding issues and idea implementations. I'm grateful for the support of my study from the Stephen and Anastasia Mysak Graduate Fellowship. Encouragements and books from Lawrence Mysak are greatly appreciated. I acknowledge this work is supported by Qu ébécois de la Recherche sur la Nature et les Technologies (FRQNT)

CONTRIBUTIONS OF AUTHURS

This thesis is based on a journal manuscript, which was submitted to the Journal of Earth and Space Science in March 2015. The manuscript is co-authored by Yi Huang, who supervised the project and conducted edits of the manuscript. The work was carried out by Ying Sun. The thesis is constituted by the manuscript, but not limited to it. Actually, the thesis can be deemed as a complementary work or extension of the original work.

ABSTRACT

In this paper, we use satellite data to test the hypothesis that deep convection moistens the lower stratosphere. Water vapor measurements from EOS-MLS and ACE-FTS over North America are binned according to the ISCCP deep convection indices. The results show that in the North American region (50-112 ℃W, 10-50 ℃N) the convection impacted samples are significantly moister than the nonimpact samples in the lowermost stratospheric layer right above the tropopause, and a drier tendency is also noticed right above this moistened layer. Trajectory modeling is used to aid the identification of deep convection-impacted water vapor samples. We find that a substantial fraction of high-concentration (>8ppm) samples at 100 hPa cannot be attributed to nearby deep convections. We also test the hypothesis that through chemical reactions enhanced SWV will cause loss of ozone, by diagnosing the profiles of ozone, CO and ClO. Although convective impact on these species is evident like in the case of water vapor, we find no correlation between water vapor and ozone that supports this hypothesis.

RÉSUMÉ

Dans cet article, nous utilisons des données satellitaires pour tester l'hypothèse que la convection profonde humidifie la basse stratosphère. Des mesures de vapeur d'eau provenant de l'EOS-MLS et ACE-FTS situées au-dessus de l'Amérique du Nord sont regroupées selon les indices de convection profonde de l'ISCCP. Les résultats montrent qu'au-dessus de l'Amérique du Nord (50-112 °W, 10-50 °N) les échantillons affectés par la convection dans la couche la plus basse de la stratosphère, tout juste au-dessus de la tropopause, sont nettement plus humides que les échantillons non affectés. De plus, une tendance plus sèche est également remarquée au-dessus de cette couche humide. La modélisation de trajectoire est utilisée pour faciliter l'identification des échantillons de vapeur d'eau touchés par la convection profonde. Nous trouvons qu'une fraction substantielle d'échantillons à haute concentration (> 8 ppm) à 100 hPa ne peut pas être attribuée à la proximité de convection profonde. Suite au diagnostique des profils d'ozone CO et CIO, nous testons également l'hypothèse que des réactions chimiques SWV accrues entraîneront une perte de l'ozone. Bien que l'impact sur ces éléments soit relié, comme dans le cas de la vapeur d'eau, nous ne trouvons aucune corrélation entre celle-ci et l'ozone qui soutient cette hypothèse.

TABLE OF CONTENTS

LIST OF TABLES

LIST OF FIGURES

CHAPTER 1
INTRODUCTION

1.1 An overview of stratospheric water vapor (SWV)

Despite its scarcity (~3-5 ppmv), stratospheric water vapor (SWV) is a climatically important atmospheric constituent due to its significant radiative and chemical impacts [Forster and Shine, 1999; Solomon et al., 2010; Anderson et al., 2012]. Recent studies have particularly addressed whether and how SWV variation may be coupled with tropospheric and surface temperatures and constitute a radiative feedback that affects climate sensitivity. Huang [2013] shows that the overall stratospheric radiative effect in coupled General Circulation Models (GCMs) may amount to 0.3 W m^{-2} K^{-1}; Dessler et al. [2013] postulate that SWV alone may result in a feedback of this magnitude and especially highlight the effect of water vapor in the lower stratosphere.

Assessment of the climatic impact of SWV is impeded by the lack of understanding of processes that control its distribution and variation. An important process, transport by the overturning Brewer-Dobson Circulation (BDC), has been long recognized [Brewer, 1949]. However, it is uncertain how factors such as temperature in the tropical tropopause layer, strength of circulation, and vertical and horizontal mixing are weighted and interactively determine SWV distribution and variation [Fueglistaler et al., 2014]. Some long-term trends in the site record (e.g. the balloon measurements taken in Boulder, Colorado) cannot be fully explained by the known factors and the abrupt decrease in global mean SWV after the year

2000 remains a mystery [Hartmann et al., 2013]. On a relevant note, it is important to bear in mind that accurately measuring water vapor at low concentrations and monitoring its global, climatic variations remains a challenge. The inter-calibration issue between different in situ instruments has been a long-standing issue [e.g. Weinstock et al., 2009]. There are also considerable systematic biases between different satellite datasets [Hegglin et al., 2013]. Moreover, regional near surface measurements and satellite data differ in terms of spatial representativeness, which potentially lead to opposite estimates of water vapor trend [Hegglin et al., 2014].

1.2 SWV and deep convection

Besides methane oxidation that mostly affects the upper stratospheric water vapor budget, another process that affects SWV is overshooting deep convection, which penetrates the tropopause and is capable of directly injecting water vapor into the lower stratosphere. This moistening effect is evident from field measurements, e.g., those of Anderson et al. [2012]. It has been postulated that this may form an effective troposphere-stratosphere water vapor transport mechanism [Fu et al., 2006]. Hanisco et al. [2007] show isotopic evidence that summertime extratropical convective storms make a considerable contribution to stratospheric water vapor over the North American continent. Although global SWV climatology from satellite observations, such as Atmospheric Chemistry Experiment-Fourier Transform Spectrometer (ACE-FTS) [Randel et al., 2012] and Aura Microwave Limb Sounder (MLS) [Schwarz et al., 2013], show prominent seasonal SWV anomalies in the Asian and North American monsoon regions that seem to corroborate the account of convective impact, SWV

and deep convection maxima are not spatially overlapped in both monsoon regions and the HDO signatures that are indicative of deep convection intriguingly differ between the two monsoon regions [Randel et al., 2012]. There is also noticeable discrepancy between the situ SWV measurements and the collocated MLS samples during moistening events [Schwartz et al., 2013]. In short, it is unclear to what extent convection may affect SWV at regional or global scales. Satellite analysis of such effect is particularly lacking.

1.3 Ozone and deep convection

Ozone is another important constituent of the atmosphere. It peaks in the stratosphere (around 30 km) while the concentration in the troposphere is very low (often around 100 ppb). The roles of ozone in the troposphere and stratosphere are quite different. On one hand, ozone is regarded as a 'good' gas in the stratosphere, which absorbs UV radiation and prevents excessive UV from reaching the surface of the Earth. While on the other hand, ozone is deemed as a 'bad' gas in the troposphere, which pollutes the air and harms living creatures.

Many factors contribute to the variation of ozone concentration. Among them the effect of overshooting deep convection is very complicated and controversial. Dynamic and chemical mechanisms compete through this process. At the tropics, where large area is covered by ocean, early modelling results have shown a decrease of ozone at UT level with the occurrence of deep convection [Pickering et al., 1993]. Later detections of extreme poor ozone region and trajectory results suggest that such decrease signal is probably caused by convective injection of clean air from low levels [Kley et al. 1996]. Solomon et al. [2005] analyze the increase of

'reduced ozone event' frequency since the late 1970s and attributes this to more frequent occurrence of deep convection. However, opposite opinions also exist. Since the subsidence induced by deep convection may bring down high concentration ozone air, it is argued that ozone at UT level should be increased. This argument is also supported by observations and modelling results [eg. Sahu and Lal, 2006; Frey et al., 2015].

At mid-latitudes, the process is even more complicated. Besides dynamic mixing of ozone, chemical processes also plays an active role. With abundant anthropological activities, air is believed to have been polluted. Pollutants including ozone precursors ,such as CO, NO_X, are transported to UT level and enhance the production of ozone [Dickerson et al., 1987]. However, the noticeable decrease of ozone and enhancements of its precursors detected during a thunderstorm over North Dakota raise the question of which process dominates [Poulida et al., 1996].

Another uncertainty is the effect of enhanced water vapor. In previous view, excessive moistening generates more HO_X, a precursor of ozone, and increases the production of ozone. However, in Anderson et al. [2012], another competing chemical mechanism is stressed. Anderson et al. [2012] argues that high concentration water vapor accelerates chlorine activation and promotes the production of ClO. ClO is an effective chemical which leads to loss of ozone. Nevertheless, Apel et al. [2012] underscore the contribution of isoprene to HO_x and weaken the influence of other reactive species. Furthermore, both HO_x and ozone are found increased during a case detected by GABRIEL, which casts doubt on Anderson et al.

[2012] theory. Lacking observation evidence, to what extent the two mechanisms influence ozone redistribution, especially at UTLS level, remains unknown.

In this paper, we firstly examine the relationship between SWV and deep convections (DC) by diagnosing satellite datasets, with a focus on the North American region (50-112 °W, 10-50 °N). Specifically, we 1) investigate the co-variations of SWV and DC, 2) examine whether SWV concentration differ with respect to DC occurrence, and 3) examine whether the high-concentration SWV samples can be explained by DCs. Then we will move on to investigate the influence of deep convection on ozone and related chemicals. The datasets and model used in our analysis will be described in the following section. Then the SWV-DC relationship diagnosed from the different perspectives will be presented. Details about the convective effect on ozone in stratosphere will be given. Discussion of the results and some conclusions will be given at the end.

CHAPTER 2
DATA AND METHODOLOGY

2.1 Water vapor data

2.1.1 EOS-MLS water vapor data

We mainly use data from Earth Observing System (EOS) Microwave Limb Sounder (MLS) aboard the NASA Aura satellite for describing SWV distribution and variation. Aura was launched in July 2004. It is a sun-synchronous polar orbiting satellite with a 1:45 p.m. equator crossing time and a period of about 100 minutes (i.e., circling the Earth about 14.5 times each day). The MLS retrieves temperature, water vapor and other trace gases by measuring the thermal emission of the atmosphere at multiple microwave bands (the 190 GHz band is used for water vapor retrieval). Due to the 25 second measurement rate, the along-track spacing of samples is about 1.5 degree or about 165 km. Water vapor retrieval is given at fixed pressure levels, from 316 hPa upward. The vertical resolution of water vapor data is about 3 km in the upper troposphere and lower stratosphere (UTLS) region that we are most interested in. Details of retrieval algorithm are given by Livesey et al. [2006]. The uncertainty range of MLS SWV data is about 20% between 316 hPa and 147 hPa and 10% at 100 hPa and stratosphere [Read et al., 2007]. The level-2 retrieval data (Version 3.3) taken during the period from Jan 2005 to Jun 2008 are used in this study. As we are especially interested in the high concentration samples, we have conducted a strict quality-control process recommended by the MLS science team [Livesey et al., 2011]. Specifically, we have used these flags to screen the

data: 1) Data points for which L2gpPrecision is set negative are removed; 2) Profiles for which 'Status' is an odd number are removed; 3) Only values falling in 316 – 0.002 hPa are used; 4) Profiles whose 'Quality' field is greater than 1.3 and 'Convergence' field is less than 2.0 are used; 5) Profiles having high or low cloud status flag bits set are removed; 6) Profiles of which concentration is lower than the minimum measurable water vapor concentration at a specific level are removed.

2.1.2 ACE-FTS water vapor data

In addition, we analyze version 3.0 SWV data from ACE-FTS, which is aboard a Canadian satellite, SCISAT, launched in August 2003 [Bernath et al., 2005]. Compared to MLS, ACE-FTS uses solar occultation in the spectral range of 750-4400 cm^{-1} to retrieve water vapor concentration. ACE-FTS has similar sampling footprint to that of MLS: about 300 km in the horizontal and 3-4 km in the vertical. One advantage of this instrument is that the isotopic composition of some species such as HDO can be made available. However, due to limitations of the solar occultation technique, ACE-FTS water vapor data are limited in spatial and temporal coverage and are much less abundant than MLS data. Hence, this dataset is used here mainly for verification of some analysis results. We will focus on the MLS results in the following sections.

2.2 Ozone and related atmospheric constituents

2.2.1 Ozone data

Ozone is another constituent this study is focused on and we continue to use the product of ozone from MLS (V3.3). The data is retrieved from 240 GHz window channel and vertical resolution is around 2.5 km at UTLS level. V3.3 data has poorer along-tracking resolution (450 km) compared to V2.2 data (~200 km). At the same time, precisions of upper stratosphere have been improved at the cost of precisions at UTLS.

We followed the suggested quality-control procedure in Livesey et al. [2011]: 1) Data points for which precision is set negative are removed; 2) Profiles for which 'Status' is an odd number are removed; 3) Only values falling in 261 – 0.02 hPa are used; 4) Profiles whose 'Quality' field is greater than 0.6 and 'Convergence' field is less than 1.18 are used; 5) Profiles of which a value less than -0.15 ppmv is encountered inside the pressure range 56-261 hPa or a value less than -0.30 ppmv is detected at 316 hPa are removed. More information about data quality and retrieval method can also be found in Livesey et al. [2011] and Livesey et al. [2008].

In this study we also investigate the distribution of CO and ClO, which are closely related with the production and consumption of ozone. Details of the MLS CO dataset and ClO dataset are given in the following parts.

2.2.2 CO data

CO, a gas mainly originateed from anthropological emissions, is an important precursor of ozone. The related chemical reaction is shown below:

$$CO + OH \xrightarrow{O_2} CO_2 + HO_2, \quad (2.1)$$

$$HO_2 + NO \rightarrow NO_2 + OH, \quad (2.2)$$

$$NO_2 + hv \xrightarrow{O_2} O_3 + NO, \quad (2.3)$$

MLS CO product (V3.3) is used through the analysis process. Data is retrieved at 10 pressure levels from 215 hPa to 0.0046 hPa. CO data has a ~5 km × ~400 km at lower stratosphere level and 5.5 km × 700 km at 215 hPa. Details of retrieval method are given in Livesey et al. [2008]. Some negative data are still are still valuable, though they only represent a relative concentration of CO. This is the same with ClO data.

We follow the quality-control procedure recommended by Livesey et al. [2011]: 1) Data points for which precision is set negative are removed; 2) Profiles for which 'Status' is an odd number are removed; 3) Only values falling in 215 – 0.0046 hPa are used; 4) Profiles whose 'Quality' field is greater than 0.2/1.1 (level lower than 100 hPa/higher levels) and 'Convergence' field is less than 1.4 are used; 5) Profiles for which 147-hPa IWC is greater than 0.008g/m^3 are removed.

2.2.3 ClO data

Concerning ozone distribution, ClO is another relevant constituent we investigated. ClO is believed to work as an efficient catalyst and decompose ozone into oxygen [Anderson et al., 2012]. The corresponding chemical reactions are shown below:

$$ClO + ClO + M \rightarrow ClOOCl + M, \quad (2.4)$$

$$ClOOCl + hv \rightarrow Cl + ClOO, \quad (2.5)$$

$$ClOO + M \rightarrow Cl + O_2, \quad (2.6)$$

$$2(Cl + O_3 \rightarrow ClO + O_2), \quad (2.7)$$

With abundant water vapor injected into stratosphere by deep convection, more ClO are generated ("chlorine activation") and result in destruction of ozone.

MLS ClO (V3.3) data is retrieved at pressure levels ranging from 147 hPa to 1 hPa. It has ~3-4.5 km vertical resolution and ~250-500 km along-track horizontal resolution. Compared to the V2.2, the averaging kernels are much sharper at all pressure levels and this enables the dataset to provide independent information of each level.

The recommended quality-control method is also given as: 1) Data points for which precision is set negative are removed; 2) Profiles for which 'Status' is an odd number are removed; 3) Only values falling in 147 –1 hPa are used; 4) Profiles whose 'Quality' field is greater than 1.3 and 'Convergence' field is less than 1.05 are used.

More information about this dataset can be found in Livesey et al. [2011].

2.3 Identification of deep convection

Here we use Deep Convective Tracking data from the International Satellite Cloud Climatology Project (ISCCP-CT) [Machado and Rossow, 1993] for the period (January 2005-June 2008) that overlap with MLS and ACE-FTS datasets. ISCCP data come from five geostationary satellites. We will use GOES-EAST data for the domain: 50 ℃W-112 ℃W; 10 ℃N-50 ℃N, because we are most interested in the North American region.

The ISCCP-CT dataset was developed to identify deep convection by analyzing image pixels of the ISCCP DX dataset [Rossow et al., 1996]. Pixels that have brightness temperatures are less than 245K are defined as Convective System (CS) and those that have brightness temperatures are less than 220K are referred to as Convective Clusters (CC). Deep convective clouds recorded range from 90 km to 350 km in size. Information including time, center position (latitude, longitude), radius and family number of each CS are provided at 3-hr time intervals and 30-km spatial intervals. Consecutive images are used to observe movement of each CS; the position and size of the CS are recorded. The same convective system detected at different time is given a same family number [Machado et al., 1998].

Here we identify DC by comparing the lowest brightness temperature (LBT) recorded in the ISCCP dataset to a threshold temperature. Different threshold temperatures have been used in previous works for such purpose [e.g., Zipser et al. 2006; Kubar et al. 2007; Yuan and Li 2009; Bedka et al. 2010]. We have tested different values ranging from 195 K to 245K at 5 K interval. The results presented below are based on a threshold value of 195 K, to ensure that the DC cases selected are overshooting cases of interest. We will discuss possible impacts of this choice wherever necessary in the rest of the paper.

Based on the information provided by ISCCP-CT data, we divide MLS data into three groups: storm, nonstorm and uncertain. Two latitude-longitude boxes are drawn here for categorizing the data. Both boxes are centered at the average center position (longitude, latitude) of each CS family within which a DC is identified. The size of the smaller box is given by the average radius of the family during its life time. The size of the larger box is the area covered

by all CSs belonging to the family. MLS data samples falling into the smaller box are identified as “storm” samples; data outside the larger box, “nonstorm” samples; the ones in-between “uncertain”. The time window used for the “storm” search is set as the life period of the CS family and the time is increased by 3 hours on both ends for “nonstorm”

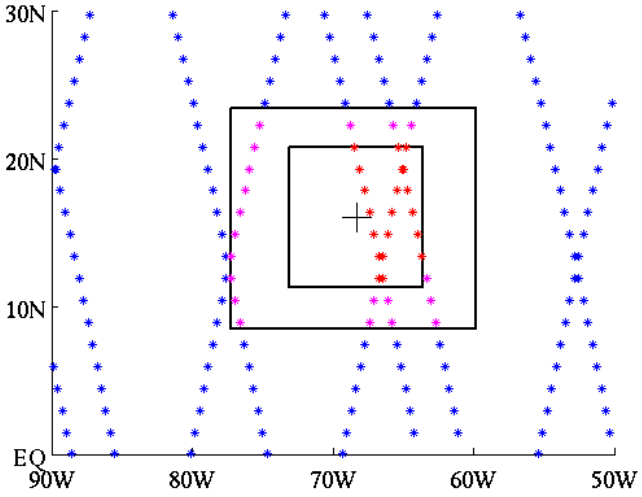

Figure 2-1. An example illustrating how SWV data are categorized. The black cross represents the average center of one CS family, which happened in October 2007. The two black boxes drawn from the CS size information are used for selecting storm and nonstorm samples respectively (see details in the text). Storm samples (within the inner box) are dotted in red; nonstorm samples (outside the outer box), in blue; uncertain samples (in-between the two boxes), in pink.

search. Fig. 2-1 illustrates an example in October 2007 of the data categorization. The same method is also applied to other gases (ozone, CO and ClO)

2.4 Application of IWC

Defined as cloud ice mass in unit volume of atmospheric air, Ice Water Content (IWC) is another mark we used to identify deep convection, especially overshooting cases. Strong updraft inside deep convections proceeds the condensation of excessive water, so High Ice Water Content (HIWC) is often believed to be closely related with strong convection and widely used as a tracer of strong convection [eg. Carminati et al., 2014].

Level-2 MLS IWC (Version 3.3) dataset is used. IWC data is retrieved at 6 vertical levels (215-83 hPa) from 240 GHz window channel with ~300 km horizontal resolution and 3 km vertical resolution. Similar to water vapor, we use the quality control recommended by Livesey et al.[2011] : 1) Only samples inside the pressure range 215 -83 hPa are used; 2) Profiles for which 'Status' is an odd number are removed.

To eliminate temporally and geographically biases caused by spectroscopic and calibration uncertainties and pick out significant cloud hit simples, the '2σ- 3σ' screen method is applied and the steps are given as [Livesey et al., 2011]:

1) IWC is averaged in every 10 °latitude bins and outliers are screened out by 2σ. Such process will be repeated until convergence is reached.

2) After Step 1) every latitude bin will be given an average (μ) and standard deviation (σ). Interpolate μ and σ to the latitude of each sample.

3) Use 3σ screen window to pick out cloud hit samples.

After those steps, measurements with the existence of convective cloud should be picked out and marked. We will use those marks to categorize other products (water vapor, ozone, etc.) and do analysis. Since the measurements of water vapor and IWC are conducted on the same satellite, most spots of measurements are overlapped. We coordinate water vapor dataset with IWC and abandon the water vapor samples without IWC measurements. This process will typically remove less than 0.0001% water vapor samples globally and is also applied to the categorization of other components.

2.5 Trajectory model

The Hybrid Single-Particle Lagrangian Integrated Trajectory (HYSPLIT), version 4, is used here. This model was developed by NOAA Air Resources Laboratory [Draxler and Hess, 1998] and has been widely used to study aerosol transport and water vapor distribution [e.g. Strong et al., 2007]. We use this model to analyze the back trajectory (historical locations) of high SWV concentration samples.

Samples are tracked on isentropic surfaces [Newman et al., 2001]. A parcel at each position is traced back up to 10 days and encounters with deep convection near the parcel locations is searched according to the same criterion used for finding storm samples above. Once a DC is encountered along the back trajectory or the trajectory extends outside the study domain (50 ºW-112 ºW), we will stop the tracking. To assess the uncertainty brought by the wind data, two reanalyses, NCEP/NCAR reanalysis 1 and Eta Data Assimilation System (EDAS40), are used here. The NCEP/NCAR reanalysis 1 provide 4 times daily data at $2.5^{\circ} \times$

2.5° horizontal resolution since 1948. The data are presented at 17 fixed pressure levels. Details can be found in Kalnay et al. [1996]. The EDAS dataset, which covers U.S. region, is on a 185x129 Lambert Conformal grid with 40 km horizontal resolution and is available at 26 fixed pressure levels ranging from 1000hPa to 50hPa at 3hr intervals. More information is provided at https://ready.arl.noaa.gov/edas40.php. Data are presented on a Lambert Conformal grid covering about 60 °W-140 °W North American region, so the longitude coverage in the tropics is lower. We only use the EDAS dataset to calculate trajectories for samples located in the 30-50 °N band, because of less overlap with the study domain in the low latitudes.

2.6 Auxiliary data

In addition to the above datasets, ERA–Interim dataset [Dee et al., 2011] is used to provide temperature profiles for calculating the environmental tropopause position defined by the WMO criterion [1957].

CHAPTER 3

RESULTS AND ANALYSIS

3.1 Convective effects on SWV distribution

3.1.1 Co-variations of SWV and DC

There are a total of 169426 MLS profiles falling into the study domain (50-112 ℃W, 10-50 ℃N) during the period of January 2005 – June 2008, which are used in this paper. Fig. 2a illustrates the zonal distribution of the MLS data at various levels within GOES-EAST view (50-112 ℃W) during the same period. Only samples with water vapor concentration greater than 8 ppm are shown here. Data are presented on the latitude-potential temperature cross-section. The potential temperature (θ) is calculated as $\theta = T(\frac{P_0}{P})^{R/C_P}$, where $R/C_p = 0.286, P_0 = 1000$ hPa, T and P are temperature and pressure observed at the same level as the SWV data. It is clear from the figure that a number of moist samples lie above the climatological tropopause (380K in the tropics and 330K/380K (winter/summer) in the mid-latitudes). These are the cases potentially related to DC. To have an overview of the distribution of high water vapor concentrations, water vapor samples located between 50 and 112 ℃W (GOES-East field of view) at 360-370K and 380-390K respectively are shown in Fig. 3-1. At 360-370K, in the North American region most high concentration samples are detected in the mid-latitudes (30-50 ℃N) (Fig. 3-1c). High water vapor concentration samples are much scarcer at 380-390K. Samples with concentration greater than 12 ppm are mostly

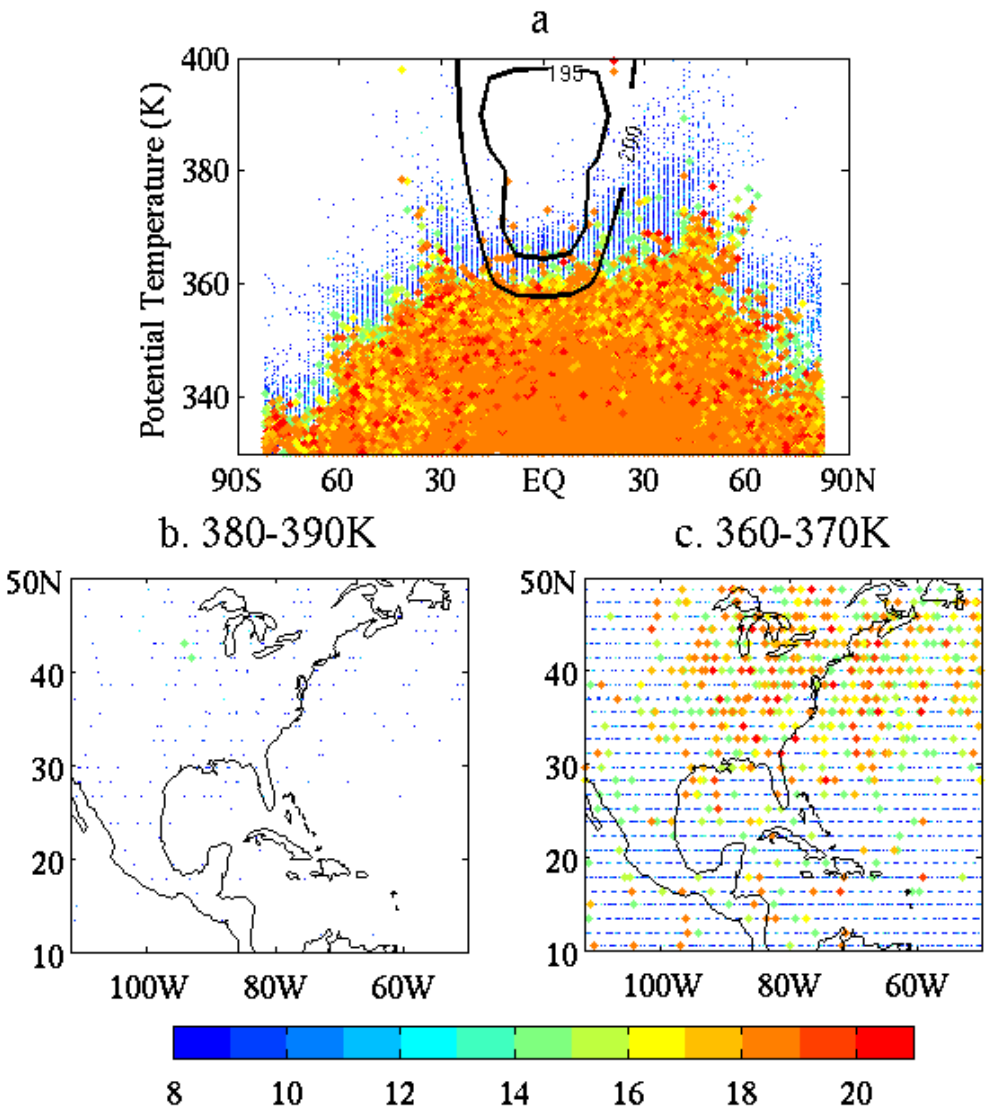

Figure 3-1. a) MLS water vapor samples presented on the potential temperature-latitude cross-section. The contour lines denote the absolute temperatures from MLS temperature profile. b) MLS samples falling into the layer with potential temperature ranging from 380 to 390 K. c) MLS samples falling into the layer with potential temperature ranging from 360 to 370 K.

located in the North American mid-latitudes (Fig. 3-1b). The fact that few high concentration SWV samples lie in the tropics agrees with the understanding that vertical transport of water vapor is subject to dehydration due to cold tropopause temperature within the tropics. [Holton and Gettelman, 2001]. Separating the samples into different seasons (not shown), we find that most of the high concentration samples (> 8 ppm) that are located above the 370 K isentropic surface and poleward to 30° latitude occur in summer. This well corresponds to the seasonality of DC activity to be discussed below.

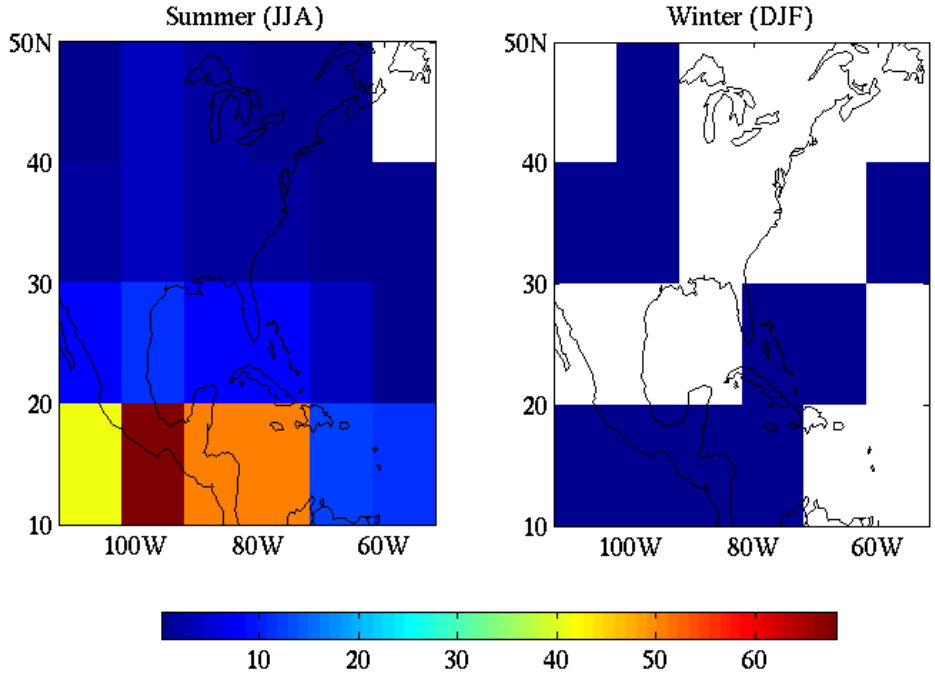

Figure 3-2. Climatology of DC frequency. Monthly counts of DC in each 10° × 10° box are denoted by different colors.

We devide the study domain into 10° × 10° grid boxes. Frequency of DC documented in the ISCCP-CT dataset of each grid box is shown in Fig. 3-2 for both summer and winter. Most convection in the study domain happen in summer, while the occurrence rate in winter is much lower (zero in many mid-latitude boxes). This is consistent with what is found in previous studies [e.g., Laing and Fritsch 2007].

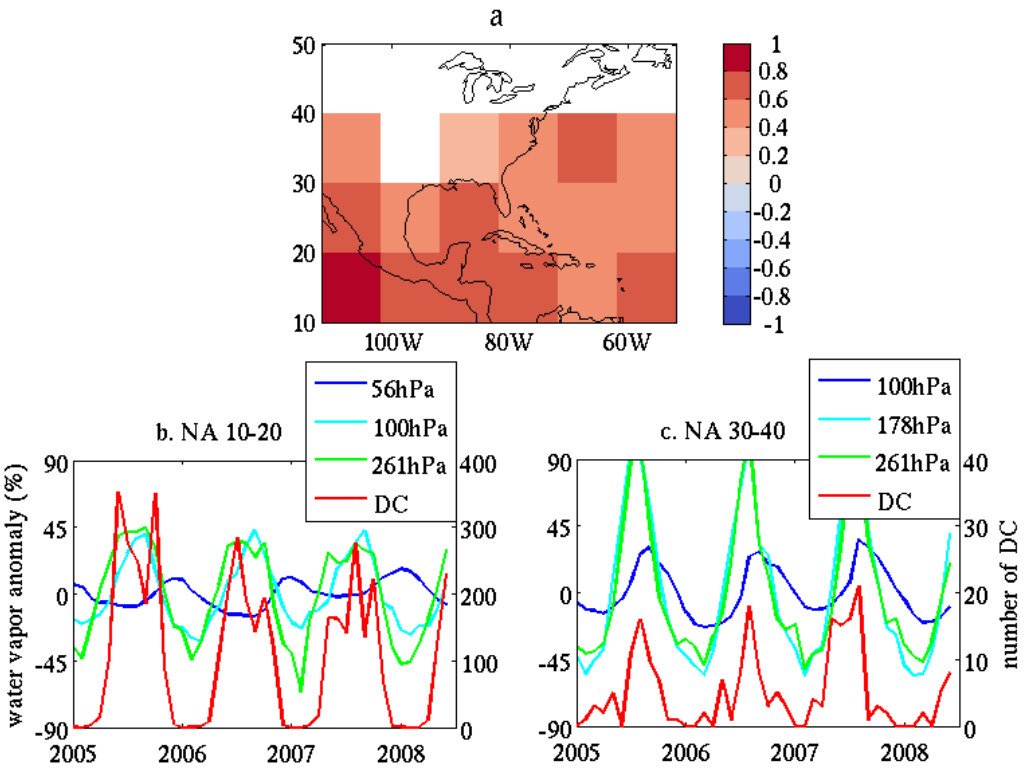

Figure 3-3. a) Correlation between 100hPa SWV and DC frequency in each 10° ×10° box within the study domain. Only the correlation coefficients that pass 95% confidence level are shown. b) Time series of SWV at a few selected levels and DC monthly count in the 10-20 ℃N latitude band; c) that in the 30-40 ℃N band.

To examine how SWV changes with DC, the correlation coefficient is calculated in each $10° \times 10°$ box between water vapor concentration and DC frequency. The correlation result at 100 hPa is shown in Fig. 3-3a. At this level, SWV is positively correlated with DC, suggesting that deep convection explains the seasonal variation of lower-stratospheric water vapor. It is also noticed that water vapor concentrations at different vertical levels vary in an unsynchronized manner. At higher vertical levels water vapor concentration tends to be anti-correlated with DC. For example, in the 10-20 ℃N band, the water vapor anomaly at 56hPa is opposite to the DC fluctuation. In the 30-40 ℃N band, a phase lag between the 100 hPa SWV and DC can also be seen.

We note that the seasonality of DC and thus the correlation between DC and SWV are sensitive to the LBT threshold for DC identification. We find that if including shallower DC using a threshold temperature higher than or equal to 210 K, the number of DC in mid-latitudes becomes higher in winter because winter cyclones frequently occur in this region. Considering that the high concentration samples in the lower stratosphere occur predominantly in summer in the region (see Figure 2 and discussions above), this means it is necessary to use a low threshold value (195 K is used here) to screen out the shallow convections irrelevant to the problem investigated here.

3.1.2 Storm vs. Non-storm profiles

We examine the influence of DC on water vapor distribution by comparing composite vertical profiles of storm and nonstorm groups categorized based on the procedure explained

in Sect. 2. Since the tropopause position at different latitudes is different, we divide the North American region (10-50°N, 50-112°W) into four 10-degree latitude bands. We calculate seasonal tropopause position based on both MLS and ERA interim temperature profiles. Both results suggest that in the low latitudes (10-30°N) tropopause does not have much seasonal variation and it is around 100 hPa. However, seasonal tropopause variation cannot be neglected in the mid-latitudes (30-50°N). The lapse rate tropopause calculated based on MLS temperature profile is at 147 hPa in boreal summer and at 215 hPa in boreal winter in the 30-40°N band, and is at 178 hPa and 215 hPa respectively in the 40-50°N band. The results calculated from ERA data are similar. So we examine vertical water vapor profiles in the 30-40°N and 40-50°N bands in summer (JJA) and winter (DJF) respectively. Results are shown in Fig. 3-4.

The impact of deep convection is very noticeable. For example, in the 10-20°N band, MLS data show significant increase in water vapor concentration in the UTLS region in the storm samples as compared to the nonstorm samples (Fig. 3-4a and b). This moistening signal is evident from the comparisons of most latitude bands.

Another noticeable feature is a dehydration signal at higher levels in the stratosphere, i.e., statistically significant decrease of water vapor concentration, e.g., around 40-60 hPa in the 10-20°N band. This signal is also observed in the other latitude bands. Using averaging kernels [Livesey et al., 2011] of MLS water vapor products, we find that moistening in adjacent moistened lower layers cannot fully explain the drying signal. This suggests that there may be physical reasons that account for the dehydration observed.

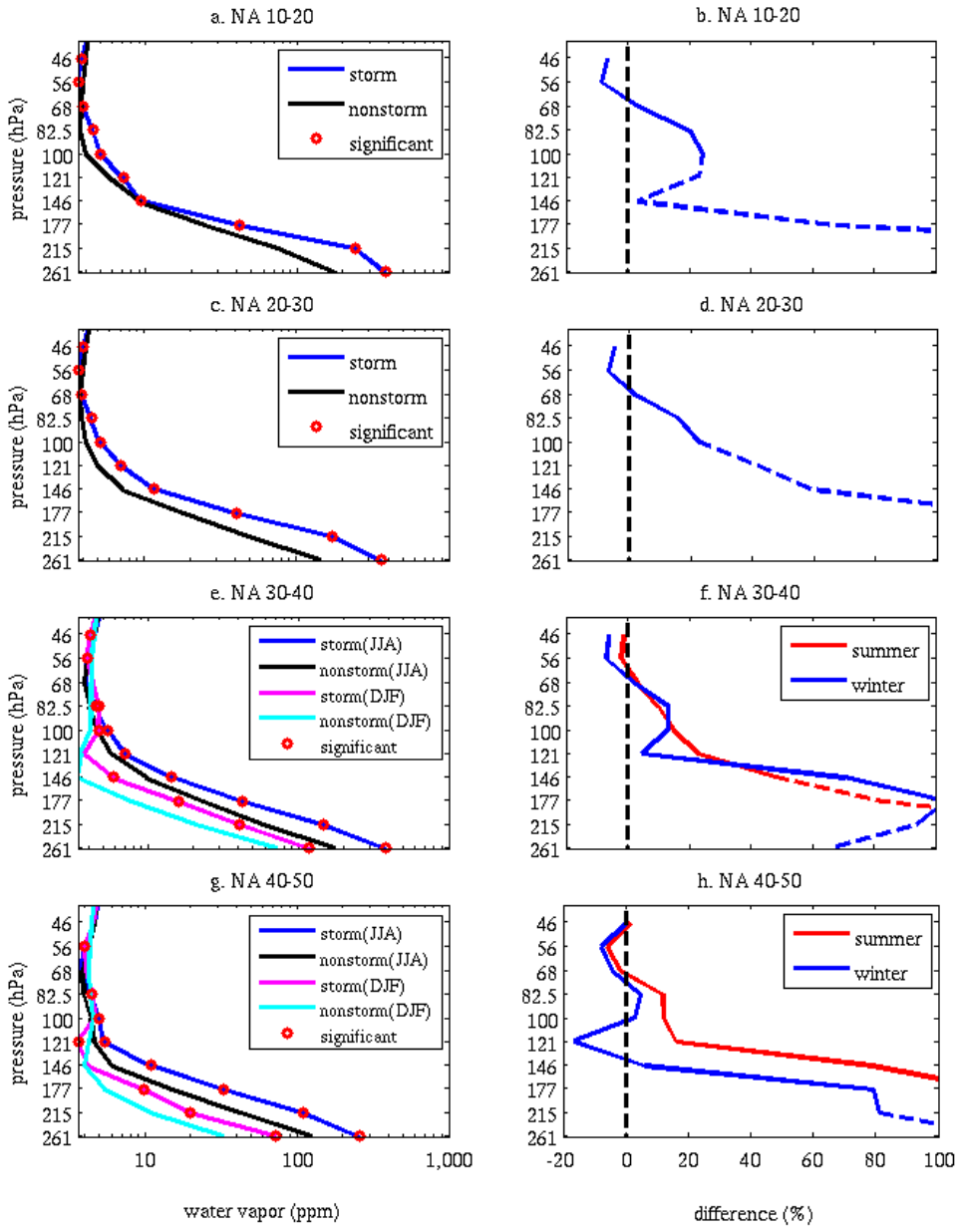

Figure 3-4. (Left column) Composite water vapor profiles of the storm and nonstorm groups in four latitude bands are shown. MLS retrieval levels are labeled. The levels where the difference passes 95% confidence level (t-test) are highlighted by red circles. (Right column) Relative difference between the storm and nonstorm samples. Solid line represents the portion of the vertical profile that is above the seasonal mean tropopause height, and dashed line, the portion below.

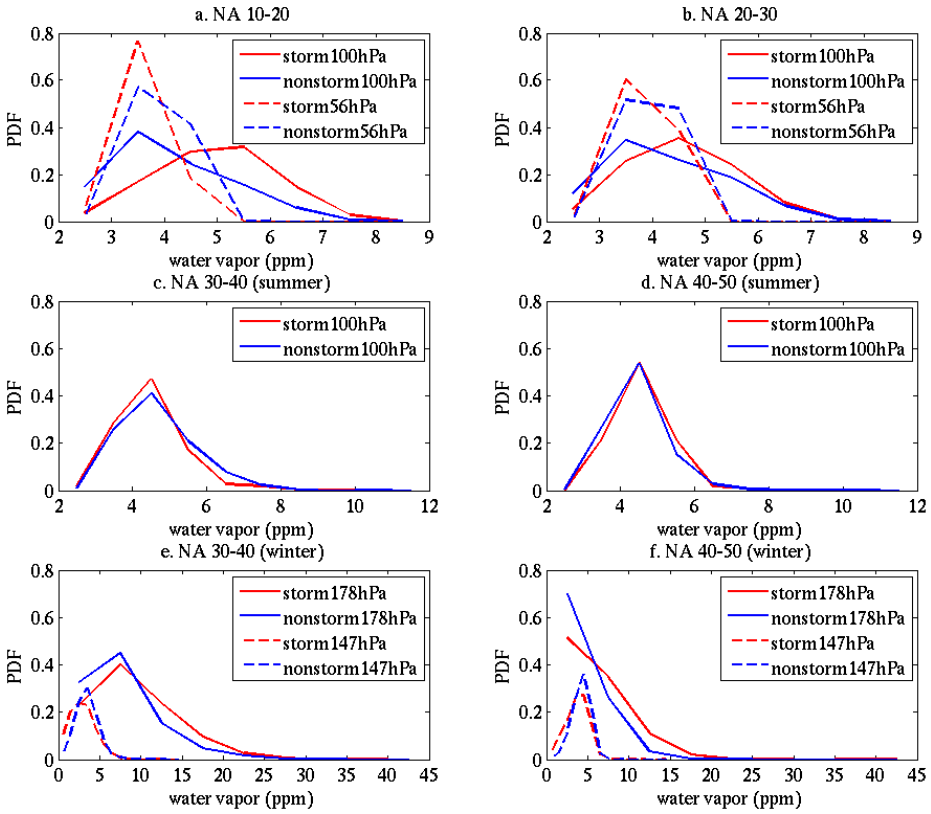

Figure 3-5. PDF of SWV at selected levels in each latitude band.

We also calculate the probability distribution function (PDF) of water vapor concentration at identified wetter (or drier) levels in different latitude bands. Fig. 3-5 shows noticeable differences between the storm and nonstorm cases. The difference is especially noticeable in the low latitude band and summertime mid-latitude bands, where concentration in the storm cases leans towards higher values than the nonstorm cases (Fig. 3-5a,b,e and f). This corroborates with the results above that DC moistens UTLS. It is widely believed that the contribution of DC to stratospheric water vapor budget is most substantial in the mid-latitudes

[Hanisco et al., 2007], and the analyses here verify the moistening effect with satellite observation evidence.

The results are verified using ACE-FTS water vapor data (not shown). The moistening-drying pattern seen from ACE-FTS data agrees well with the MLS results in most cases except that the position of dry signal derived using ACE data is a bit higher than that derived using MLS data in the mid-latitudes. This is likely due to the different vertical coordinates used in retrieval for the two satellites [Hegglin et al., 2013].

3.1.3 Effects of DC capped at different levels

Deep convections may reach different vertical levels decided by their strengths and environmental conditions. Those who can pierce the threshold of tropopause and overshoot into stratosphere are defined as overshooting events, which are believed to have significant influence on SWV distribution especially.

As discussed in the previous sections, DC identification (storm sample selection) is subject to the threshold LBT used in this study. A range of threshold values is tested. To minimize the impact of shallow (non-overshooting) convection on the storm composite, a rather low value 195 K has been used for most of the results presented in this paper. On the other hand, the nonstorm composite is little impacted by this criterion owing to the much larger sample size. In general, the storm-nonstorm difference remains a moister UTLS layer overlaid by a drier layer, although the moistening in the lower stratosphere (at the MLS retrieval levels above the tropopause) becomes indiscernible in mid-latitudes (30-40 ℃N) when

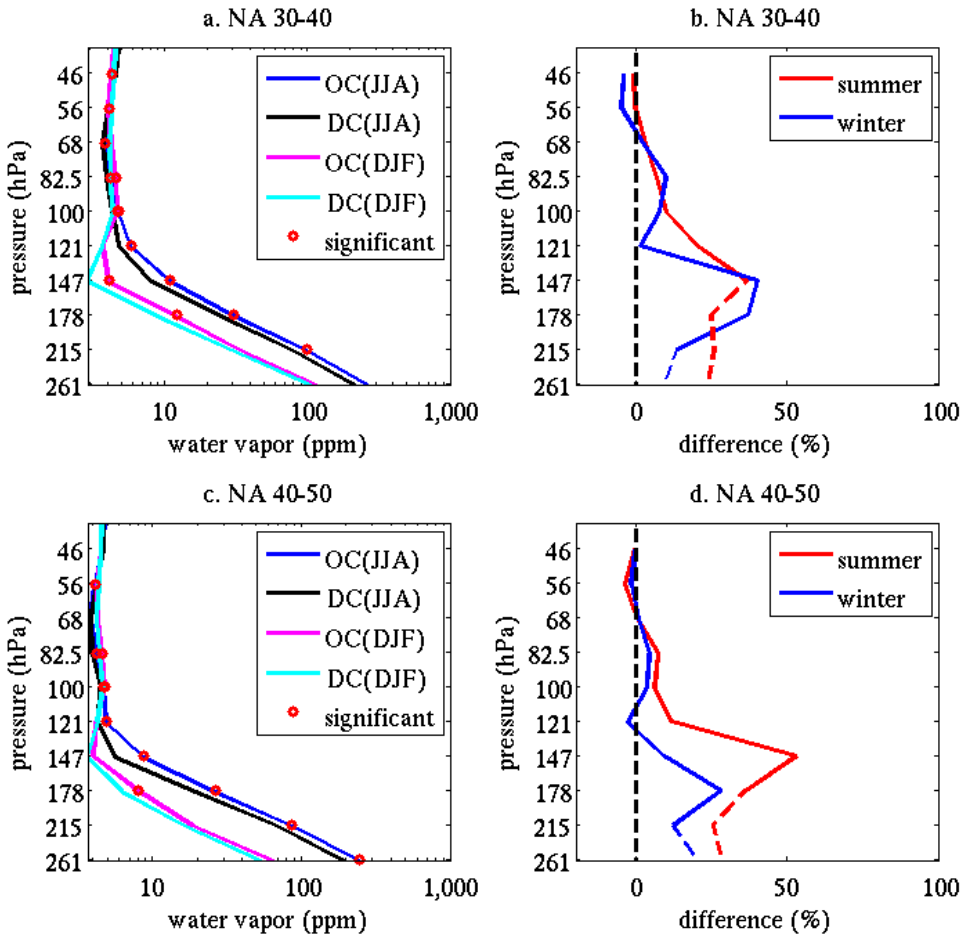

Figure 3-6. (Left panels) Composite water vapor profiles of overshooting convection (OC) and DC in the 30-40 ℃N and 40-50 ℃N bands. OC represents a subset of deep convection-impacted samples with cloud top temperature less than 200K and DC represents the rest of the convection-impacted samples. The levels where the differences pass the 95% confidence level in a t-test are marked by red dots. (Right panels) Fractional differences.

LBT threshold higher than 210K is applied. In addition, we notice that the level that separates the drier upper layer from the moister lower layer goes upward when colder LBT threshold is used, which suggests that stronger overshooting deep convection "pushes" both moistened and dehydrated layers upward. Modeling results showed that high-capped DCs are more likely to moisten high stratosphere levels [Dessler et al., 2007]. Our analysis provides observational evidence for this argument.

To further examine the effect of overshooting events and compare with the results stated before, another categorization mark IWC is used. Strong deep convection with speeded updraft are able to penetrate tropopause and excessive water vapor inside is condensed out into ice. So the amount of ice in a unit air is a good tracer to identify overshooting events and observations have also proven its feasibility [Iwasaki et al., 2012].

Significant IWC signal is picked out through the procedure described in Sect. 2. If a significant signal is detected at tropopause in the four latitude bands respectively (100 hPa, 100 hPa, 121/178 hPa, 147/178 hPa), the corresponding samples will be categorized as cloudy group and leave the rest as noncloudy. Fig. 3-7 shows the vertical water vapor profiles of the two groups and the relative difference between them. Except 30-40 ºN latitude band, the result agree well with that of deep convection identified using ISCCP dataset (Fig. 3-4) in all the latitude bands. A moistened lower stratosphere is seen with a dry signal right above. And the levels of dry and moisten signal detected are also the same with Fig. 3-4.

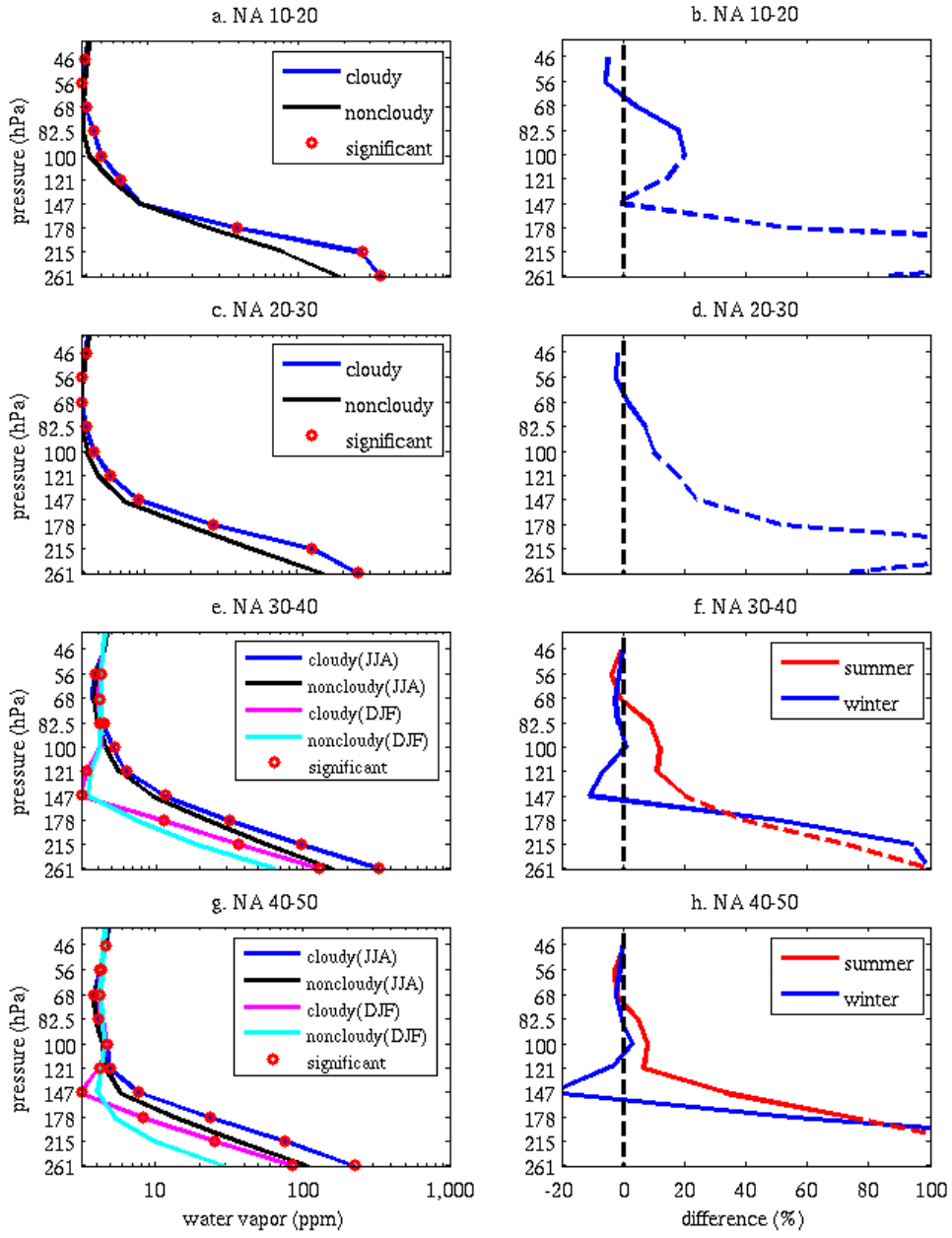

Figure 3-7. (Left column) Composite water vapor profiles of the cloudy and noncloudy groups in four latitude bands are shown. MLS retrieval levels are labeled. The levels where the difference passes 95% confidence level (t-test) are highlighted by red circles. (Right column) Relative difference between the cloudy and noncloudy samples. Solid line represents the portion of the vertical profile that is above the seasonal mean tropopause height, and dashed line, the portion below.

Although high IWC is proven to be associated with deep convections, there is still the concern that other undiscovered process may contribute to a non-convective HIWC. And the less than 50% overlapped storm and cloudy samples seem to be an evidence. So we use a joint of ISCCP and IWC to locate overshooting deep convection. As discussed in Sect. 2, ISCCP detects deep convection by observing convective cloud. If significant IWC is observed at convective cloudy regions, it is more likely that the HIWC is generated by overshooting events. The new results derived using the joint mark and IWC results are alike (not shown here), which suggests that the extreme big values of water vapor observed at 100 hPa in the summertime mid-latitudes are most probably caused by overshooting events and weaker deep convections have an opposite effect on this layer (eg. LBT>210K).

3.1.4 Trajectory analysis

As shown by Schwartz et al. [2013], most high concentration lower stratospheric water vapor samples are concentrated in the North American and Asian monsoon regions. If these high concentration samples are due to convective injection, it is expected that the samples are located within a reasonable time-space window around deep convection. Table 3-1 shows how the samples binned by their concentration values are divided into the storm and non-storm groups. Interestingly, we find that a substantial fraction of the moist samples cannot be explained by collocated deep convection. For example, at 100hPa half of the >8 ppm samples (137 out of 166 samples) belong to the nonstorm group, almost double that in the storm group (13 out of 166). A possible explanation that explains this is possible long-range transport of

high water vapor concentration air parcels. Here, this effect is analyzed using the HYSPLIT trajectory model.

All samples with concentration greater than 8 ppm in the North American region (10 ℃N-50 ℃N, 50 ℃W-112 ℃W) at 100hPa are selected and set as the initial point to calculate back trajectories. With 20, 53, 47, 17 samples in each latitude band, a total of 137 samples are examined in the trajectory analysis. Most of these samples are over the continent.

Table 3-1. Number of samples of Storm and Nonstorm groups falling into different concentration bins at different latitudes.

Latitude Band	Group	<2	2-3	3-4	4-5	5-6	6-7	7-8	>8
10-20°N	Storm	0	32	174	362	386	193	34	8
	Nonstorm	133	5291	14074	8449	5170	1962	258	20
20-30°N	Storm	0	7	49	126	144	73	16	3
	Nonstorm	110	4662	15023	10565	6924	2465	376	53
30-40°N	Storm	0	1	23	35	28	15	2	2
	Nonstorm	27	1557	12973	14818	7715	1859	293	47
40-50°N	Storm	0	0	20	46	16	3	1	0
	Nonstorm	0	272	8386	22475	7674	758	76	17

Since parcel release position influences trajectory result and there is uncertainty in the position of MLS samples (mainly due to its low vertical resolution), we calculate trajectories at multiple vertical levels (16, 16.5, 17, 17.5 and 18 km) around the level (100 hPa) where each sample is reported. As discussed in Sect. 2, parcels are traced back at 48-hr intervals up to 10 days. CSs that happened during the period are searched to determine whether each sample

encountered DC. Here we define the influence region of one CS by the radius of each CS documented in the ISCCP dataset. To simplify the procedure, 100 km is approximated as 1 °. The search domain is enlarged by 1 ° in addition to account for the uncertainty in the CS influence region. If the trajectory crosses any CS influenced region, the high concentration sample is tagged as "explained" by DC. For example, on 7 August 2005 8:00:00 UTC a high concentration sample is detected at (17.8 ℃N, 97 ℃W). We trace back from this position and analyze back trajectories in five 48-hr segments. As shown in Fig. 3-8, the hourly positions of the parcel are recorded and the CSs that happened during the time are marked. In this case, 2

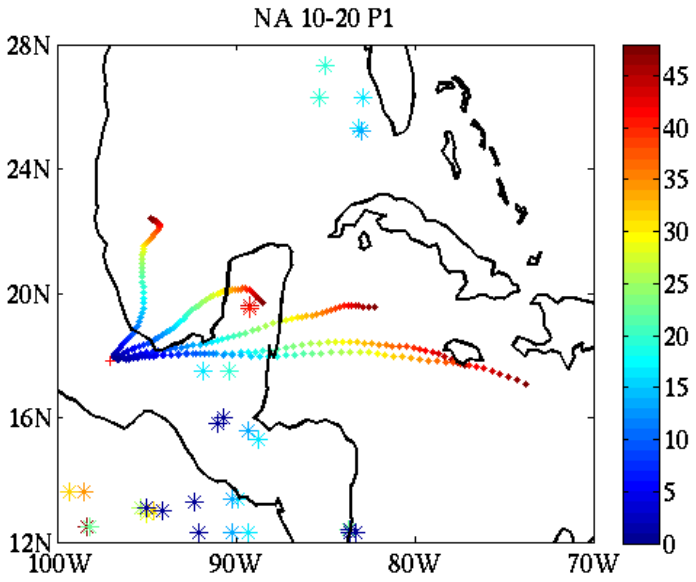

Figure 3-8. An illustration of the trajectory analysis. One high-concentration sample is observed at (17.8 ℃N, 97 ℃W) in August 2005 (marked by a red cross). From this initial position, the back trajectories in the first 48 hours are shown here. The hourly positions are denoted by different colors. DCs that happened during the 48 hours are color-coded in the same way. Then historical encounters with DC is determined by the distance between the sample position and DC location(s) at the same time.

locations at 19 ℃N that happened 45 hours ago and 2 CS locations at 17 ℃N that happened 20 hours ago are found. This high concentration sample will be regarded as being explained by DC within 20 hours in history.

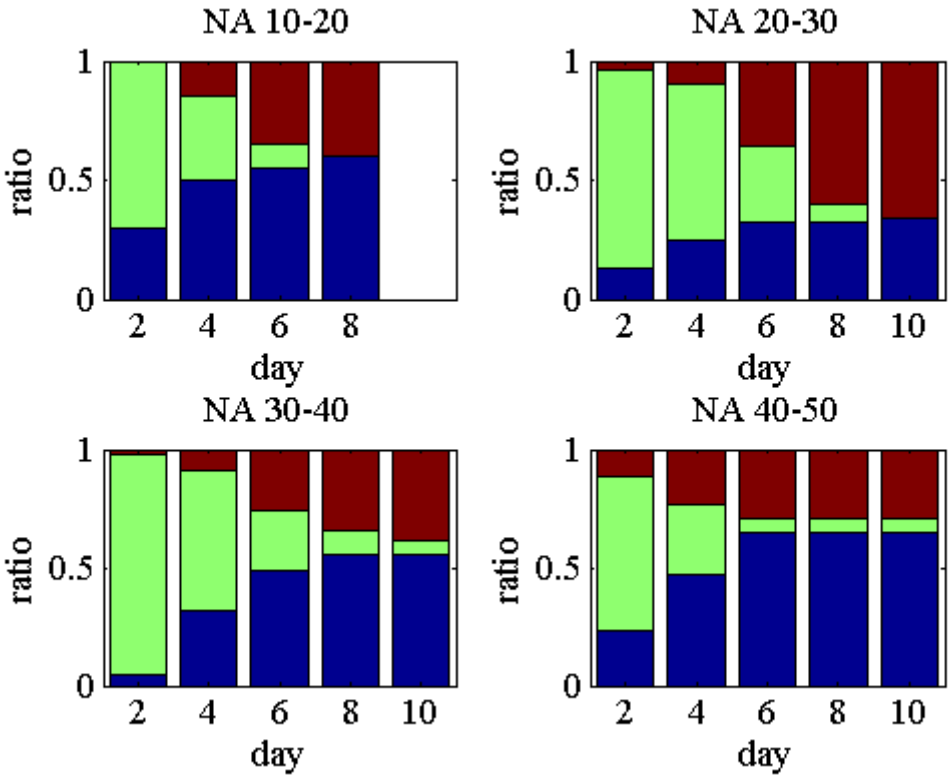

Figure 3-9. Ratio of high-concentration samples explained by DC. The horizontal axis shows the time of back tracking and vertical axis is the ratio. Blue bars show the ratio of samples that are explained by DC. Red bars, that of samples whose trajectories extend outside the study domain without encountering any DC. Green bars, that of samples whose trajectories are still within the domain but without encountering any DC. The results are based on the trajectories derived from NCEP/NCAR reanalysis data.

Following this procedure, each sample in the four latitude bands is traced back to search for DC encounters. Results derived using NCEP/NCAR reanalysis data are summarized in Fig. 3-9. In the 10-20 ℃N band, the tracking process is stopped at 8 days when there are no samples whose trajectory remains inside the domain with no DC encountered. Trajectory results explain 12 of the 20 samples in this band (Fig. 3-9a). In comparison, 18/53 in the 20-30 ℃N band, 26/47 in the 30-40 ℃N band, and 11/17 in the 40-50 ℃N band are explained (Fig. 3-9 b, c and d). In summary, only a fraction of these moist samples can be explained by DC; the unexplained samples amounts to 70, more than 40% of all the moist samples (a total of 166). Results derived using the EDAS data are similar (not shown).

Note that we have adopted a strict criterion (195 K threshold) for selecting DC and thus may have underestimated the likelihood of DC encountering. To examine this uncertainty, we relax the criterion to 245K and re-search for DC along the trajectory. As a result, now more than 80% samples can be explained in the 10-20 ℃N and 40-50 ℃N bands. However, the ratio has little change in the 20-30 ℃N and 30-40 ℃N bands; there are still about 30% samples that cannot be explained. Furthermore, each sample is traced back at 5 vertical levels and if any of these 5 trajectories encounters DC, the sample is categorized as explained. But despite all the reasons that may have led to overestimation of DC encountering likelihood, a number of anomalously high concentration samples cannot be explained neither by local vertical transport nor long-range transport (up to 10 day and within the study domain).

3.2 Convective effects on UTLS ozone distribution

We use MLS ozone (V3.3) data to investigate the influence deep convection exerts on UTLS ozone distribution in the North America region (10-50 ℃N, 50-112 ℃W). MLS ozone data shows that ozone peaks at 10 hPa and the maximum can be as high as 12 ppm. Figure 3-10 provides a whole picture of 10 hPa ozone distribution in American region. At this level, tropical region, where sunlight is intense, favors high concentration ozone samples. Comparatively low concentration samples are observed in the two Polar Regions. Seasonal variation is believed to be related to sunlight intensity and circulations which realize long-range ozone transport [Wardle, 1997]. On the contrary, at 100 hPa ozone concentration peaks in the Polar Regions while the concentration in the other latitudes is usually less than 1 ppm (not shown). Because excessive loss of zone occurs at 35-45 km, 10 hPa is a critical layer of ozone hole studies. But in this paper, we will focus on the ozone variation at UTLS, which is subject to the impact of deep convection.

We use the same method explained in Sect. 2 to categorize the North American ozone samples into storm and nonstorm groups, and cloudy and noncloudy groups. Fig. 3-11 shows the comparison between storm and nonstorm group. To minimize noises, only levels where the difference passes 95% t-test is plotted in the right column. Due to the convective transport, there is a decrease in ozone concentration in the UTLS. It is interesting that such decrease signal appears to reach different altitudes in different zonal bands. In the low latitude bands (10-20 ℃N and 20-30 ℃N), the decrease signal is capped below 100 hPa and limited in the upper troposphere (Fig. 3-11b and d). Whereas, in the mid-latitudes (30-40 ℃N and 40-50 ℃N), the

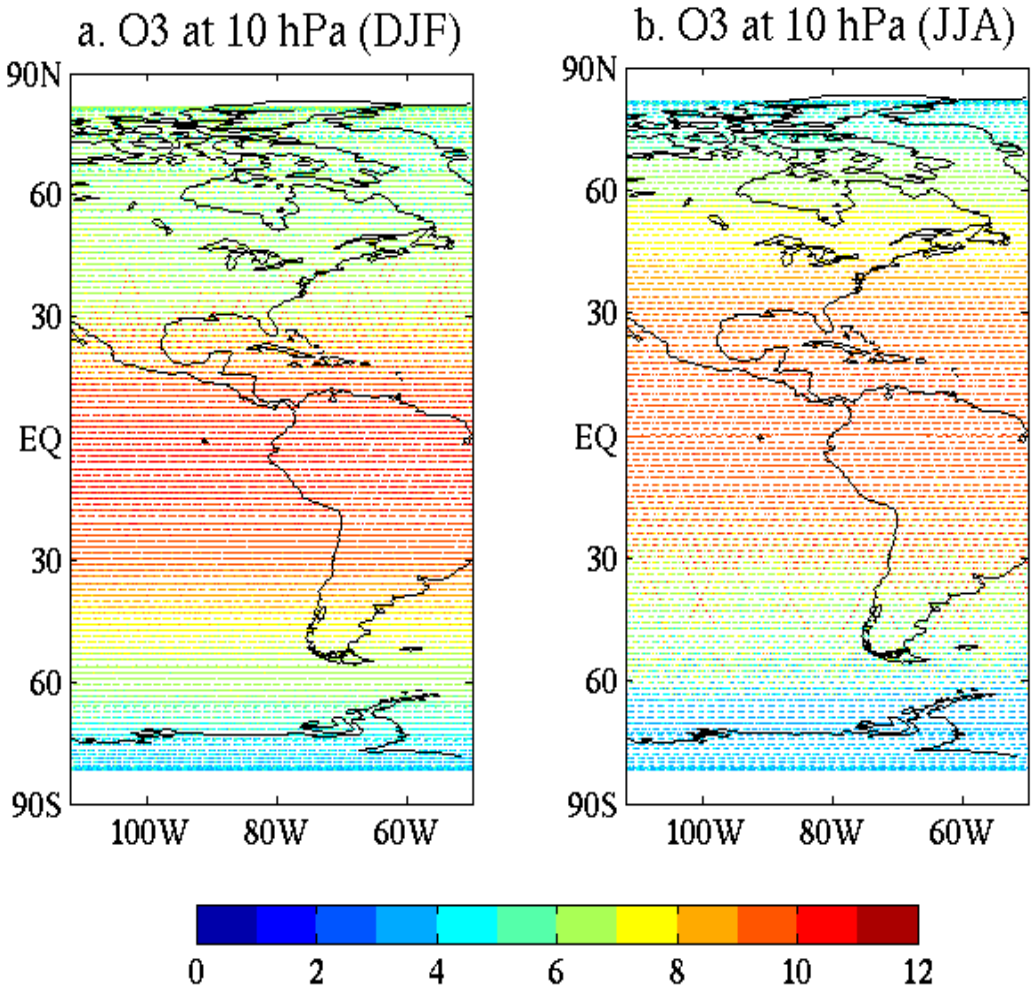

Figure 3-10. 10hPa MLS ozone samples of boreal winter (left) and boreal summer (right).

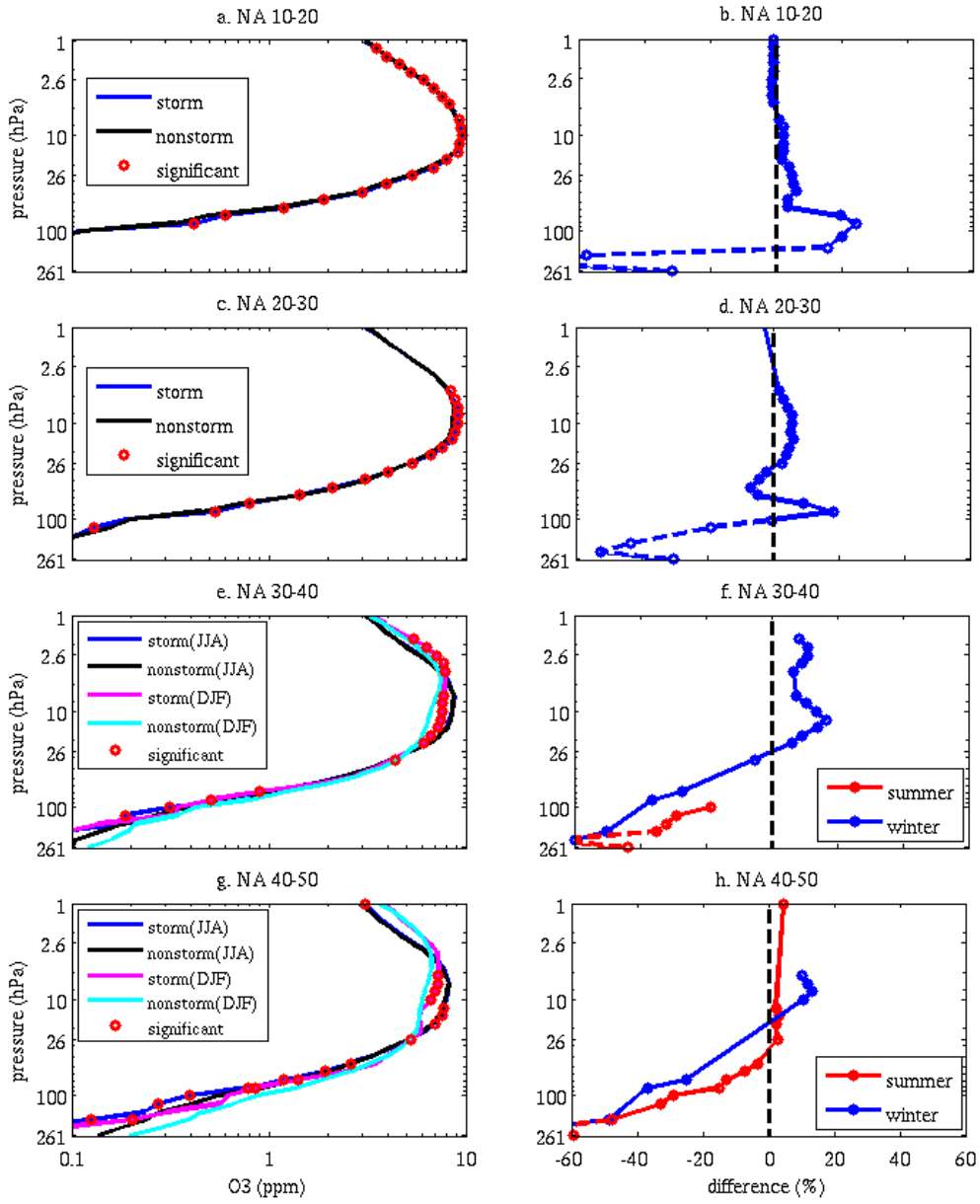

Figure 3-11. (Left column) Composite ozone profiles of the storm and nonstorm groups in four latitude bands are shown. The levels where the difference passes 95% confidence level (t-test) are highlighted by red circles. (Right column) Relative difference between the storm and nonstorm samples (levels where the difference is not significant are ignored). Solid line represents the portion of the vertical profile that is above the seasonal mean tropopause height, and dashed line, the portion below.

decrease signal can reach as high as 30 hPa (Fig. 3-11f and h). In general, an increase is found at the layer immediately above. Results derived using IWC indicators are similar except that no increase signal is detect at mid-latitudes (not shown).

The UTLS decrease signal in the tropical region (10-20 ℃N and 20-30 ℃N) is expected. North American tropical region is mostly covered by ocean. Deep convection brings clean air from marine boundary up to UTLS and dilutes ozone density at this level [Kley et al., 1996]. Although it is suspected that deep convection may sometimes inject polluted air with abundant ozone precursors into UTLS [Dickerson et al., 1987] and enhance ozone concentration at mid-latitudes, the observations analyzed here show no evidence of such effect. Moreover, the zonal difference of ozone variation is also an evidence of vertical transport theory.

Anderson et al. [2012] argue that enhancements of water vapor over the United States by deep convection accelerate the chlorine activation and finally cause excessive loss of ozone in the lower stratosphere. ClO is a key compound to induce the catalytic reaction and reduce ozone concentration (Sect. 2.2.3). This theory has been testified in polar region and upper troposphere [eg. Vogel et al., 2006; Rodriguez et al., 2012], but not been proved for the LS level. Since a decrease signal is observed at UTLS level in our study, we continue to test Anderson's hypothesis and investigate ClO's contribution to this decrease signal. Following the same procedure described in Sect. 2.3 and 2.4, we categorize MLS ClO data into storm, nonstorm, cloudy and noncloudy groups. Both ISCCP results and IWC results present an

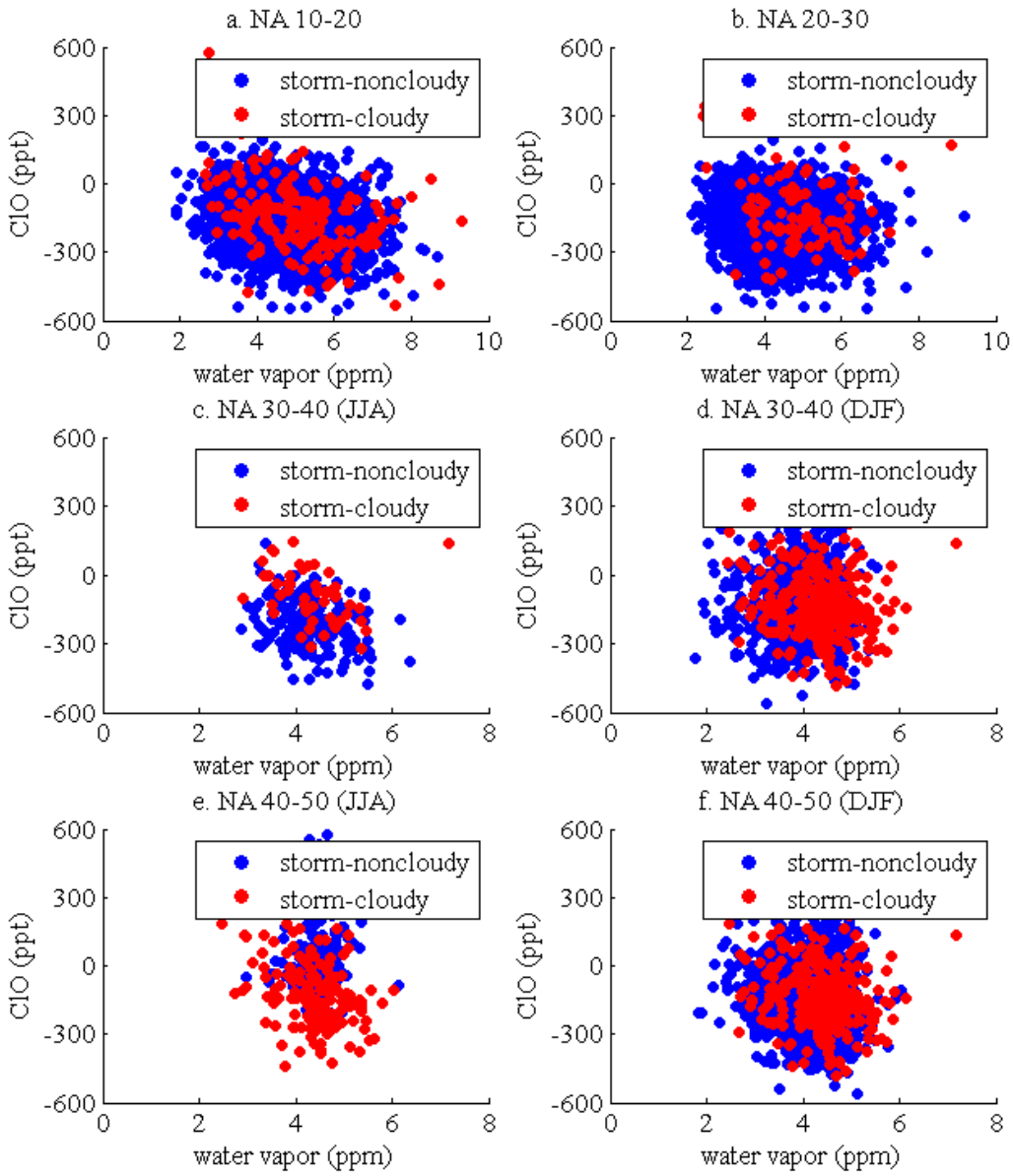

Figure 3-12. At each spot, a measurement of water vapor and ClO is made. Water vapor and ClO of storm-noncloudy and storm-cloudy at 100 hPa is presented here.

Increase of ClO through the UTLS, which is inconsistent with the ozone vertical profile, in all the latitude bands. We also study the 100 hPa water vapor and ClO samples to check the correlation between them. Following Anderson's hypothesis, a positive correlation is expected. However, the correlations vary in different latitude bands. Because ice is a necessity for heterogeneous reactions in Anderson's hypothesis, we further study the correlation between ClO and water vapor of storm-cloudy and storm-noncloudy groups. Instead of a positive correlation, an anticorrelation is seen (Fig. 3-12).

The ozone increase signal above the decrease layer remains a puzzle. It is thought that the chemical reaction discussed in Sect. 2.2.2 may be a possible mechanism which contributes to the increase of ozone. On one hand the enhancement of ozone precursors like NO_X and CO promotes the production of ozone [eg. Hingane, 1989; Wang et al., 2014] ; On the other hand, increase of water vapor leads to faster generation of HO_X and may also result in an increase of ozone. To examine this thought, we compare the storm, nonstorm, cloudy and noncloudy composite profiles of CO. Results are given in Fig. 3-13. The main source of CO is in the troposphere, so the vertical distribution of CO is similar to that of water vapor. It decreases with altitude below 30 hPa and then increases slowly upward. Regardless of different tropopause conditions, CO is increased below 147 hPa and decreased around 100 hPa in all the four latitude bands. The same trend is also seen in IWC results (not shown). However, the levels where the CO signals are observed are not consistent with ozone profile. We note that CO and ozone are retrieved at different levels (37 vs. 55, see details in Sect. 2), so that inconsistency may originate from this.

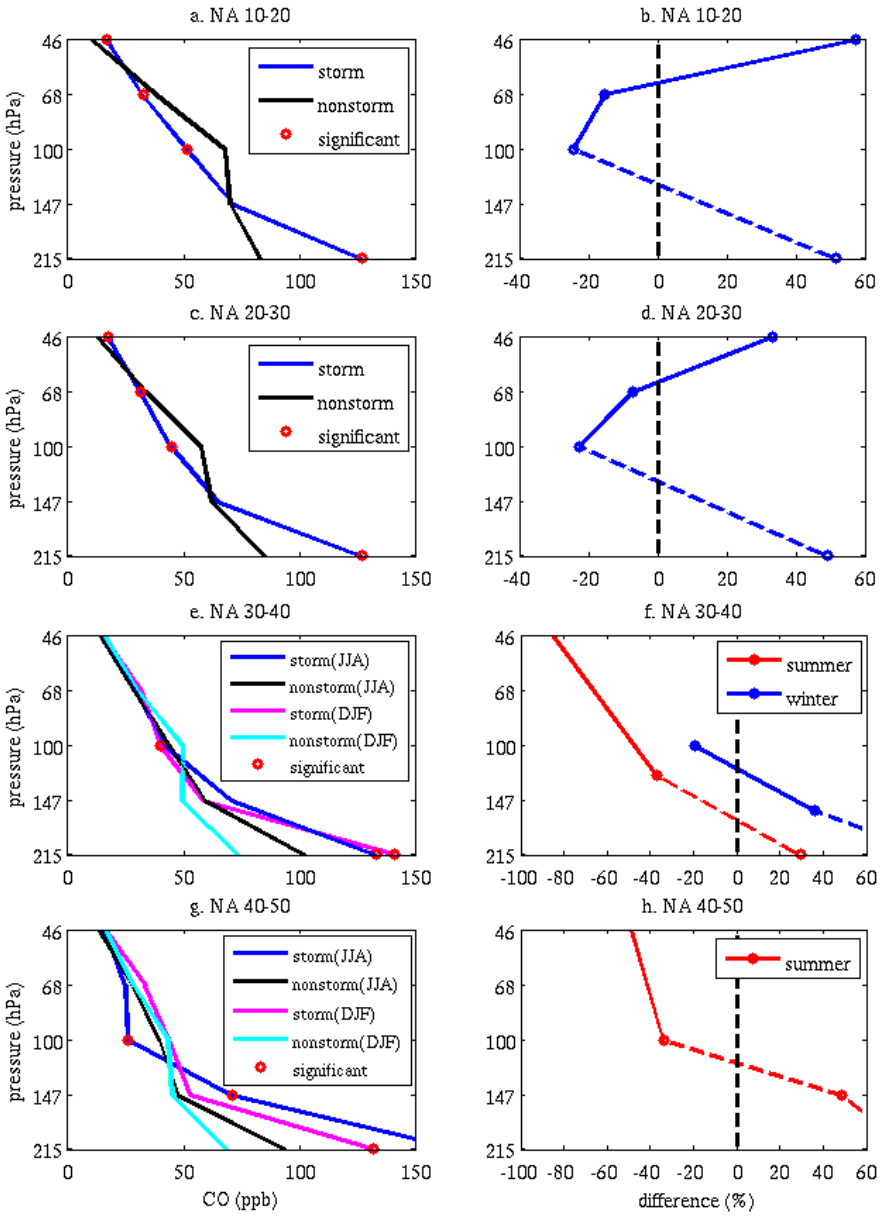

Figure 3-13. (Left column) Composite CO profiles of the storm and nonstorm groups in four latitude bands are shown. The levels where the difference passes 95% confidence level (t-test) are highlighted by red circles. (Right column) Relative difference between the storm and nonstorm samples(levels where the difference is not significant are ignored). Solid line represents the portion of the vertical profile that is above the seasonal mean tropopause height, and dashed line, the portion below.

Moreover, correlation between CO and water vapor does not fully support the hypothesis (Fig. 3-14). In the hypothesis, water vapor raises the amount of HO_X and HO_X acts with CO to produce ozone. Hence, an anticorrelation between CO and water vapor is expected. A weak anticorrelation is indeed seen in the low latitude bands (Fig. 3-14a and b) and storm samples in the mid-latitudes (Fig. 3-14 c, d, e and f). However, there is no correlation detected from mid-latitude nonstorm samples. Such diverse correlations are also discovered in other works [eg. Livesey et al., 2013], which suggests that the correlation between ozone and CO cannot be expressed as a simple function and spatial correlation difference should be taken into consideration in future modelling development.

Admittedly, since we only study the collocated examples (winthin 3-hr time window), we may underestimate activation time of ClO and reaction time between CO and water vapor. But based on the present results, dynamic process is likely to play a dominant role for the UTLS layer. Noticing the increase signal is a bit lower than the peak of ozone, it is likely that the air that has high concentration ozone is brought downward by the subsidence induced by deep convection. This hypothesis can be tested in future work.

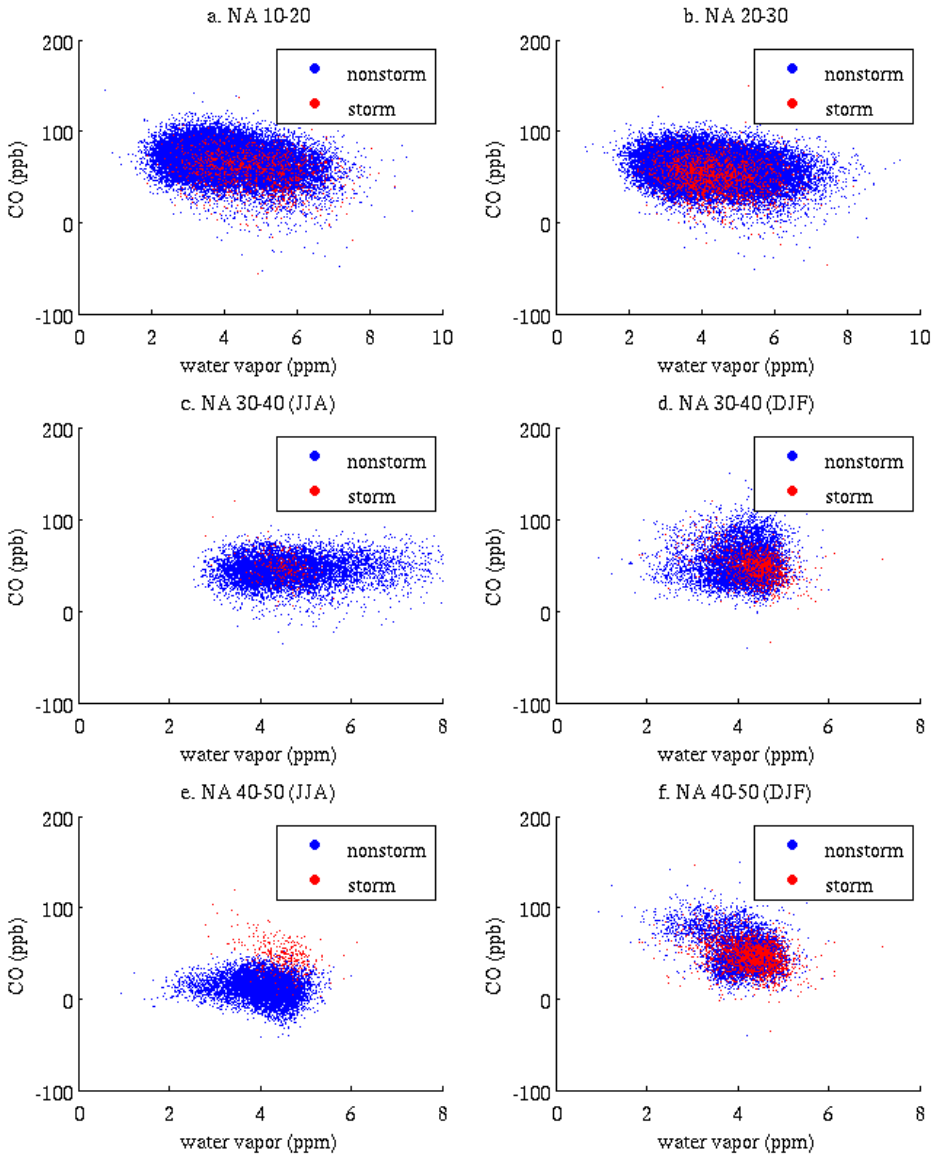

Figure 3-14. Each dot represents a collocated measurement of water vapor and CO. Water vapor and CO of each spot at 100 hPa is presented here. Nonstorm and storm samples are denoted by blue and red dots respectively.

CHAPTER 4
CONCLUSIONS

Using ISCCP Convective Tracking data to identify deep convection, we investigate the influence of deep convection on the UTLS water vapor. We first compare MLS and ACE-FTS water vapor samples collocated with deep convection to those not collocated with deep convection. A typical pattern of a moistened UTLS layer overlaid by a drier upper layer is observed in both tropics and mid-latitudes. However, in summertime mid-latitudes (e.g., the 30-40 ºN band), the convective moistening is not as prominent in the lower stratosphere as in the other cases but is limited to the troposphere. We have also calculated the PDF of water vapor concentration at different UTLS levels, which corroborate the above results.

The drying signal above the moistened layer is interesting and was also identified by other studies [e.g. Ray and Rosenlof, 2007]. Our analysis based on the MLS weighting function suggests that this is not a spurious signal due to the vertical resolution of the retrieval data. The physical cause of this signal still eludes us and warrants further study.

It is found that many high concentration water vapor samples cannot be explained by local deep convection. Using a back-trajectory model we investigate whether these samples can be caused by historical encounters with deep convection and long range transport. Back trajectories are calculated by HYSPLIT model, using NCEP/NCAR and EDAS wind data. The attribution results derived from the two datasets are in good agreement. When tracked backward longer in time, more samples can be attributed to deep convections that happened

along the trajectories.

However, even when a relaxed criterion is used for determining the convective impact on the samples, a substantial fraction of samples, especially in the mid-latitude bands, cannot be traced to any deep convection within the tracking domain (the North American region within the GOES-EAST field of view) and the time window (10 days). This may due to small-scaled convections (radius less than 90 km) that are not observed by ISCCP data. Another plausible explanation is that these moist samples are due to longer range (and time) transport. Pinning down the cause of these samples is beyond the scope of this paper but is an interesting topic for future work.

Since there are still uncertainty about the selection of LBT to define DC, we continue to modify the threshold to study the convective effect of deep convection capped at different levels (190K-245K). We found the mid-latitude results are influenced most. With the decrease of brightness temperature threshold, the moistening signal can reach higher levels and the overlaid dry signal is also push upward. When the brightness temperature threshold decreases to 200K, we found the difference between the storm and nonstorm profiles are similar to that of low latitudes (10-20 ℃N and 20-30 ℃N). However, if the threshold is set above 210K, significant dry signal begins to appear at mid-latitudes, especially in the 30-40 ℃N latitude band. Results derived using IWC, which is widely used as a tracer of overshooting, present a similar signature to the results derived using LBT lower than 200K. All of these suggest that high water vapor signal observed at 100 hPa at mid-latitudes are probably caused by strong overshooting events, and weak convection are only able to influence lower levels.

Anderson et al. [2012] argue that enhancements of water vapor will exacerbate the loss of ozone through accelerating “chlorotic activation”. We investigate the convective effect on ozone and chemical processes related to water vapor and ozone. Ozone, ClO and CO samples are categorized as storm, nonstorm, cloudy and noncloudy groups using the same method for water vapor. Diverse correlations between CO, ClO and water vapor are found in different latitude bands, which suggests that the chemical reactions in question do not explain the observed variations of ozone.

REFERENCES

Anderson, J. G., D. M. Wilmouth, J. B. Smith, and D. S. Sayres (2012), Ne, *Science*, **337**, 835-839, doi: 10:1126/science.1222978.

Apel, E. C., Olson, J. R., Crawford, J. H., Hornbrook, R. S., Hills, A. J., Cantrell, C. A., Emmons, L. K., Knapp, D. J., Hall, S., Mauldin III, R. L., Weinheimer, A. J., Fried, A., Blake, D. R., Crounse, J. D., Clair, J. M. St., Wennberg, P. O., Diskin, G. S., Fuelberg, H. E., Wisthaler, A., Mikoviny, T., Brune, W., and Riemer, D. D. (2012), Impact of the deep convection of isoprene and other reactive trace species on radicals and ozone in the upper troposphere, *Atmos. Chem. Phys.*, **12**, 1135-1150, doi:10.5194/acp-12-1135-2012.

Bedka, K. M., J. Brunner, R. Dworak, W. Feltz, J. Otkin, and T. Greenwald (2010), Objective satellite-based overshooting top detection using infrared window channel brightness temperature gradients, J. Appl. Meteor. And Climatol, 49, 181-202.

Bernath, P. F., et al. (2005), Atmospheric Chemistry Experiment (ACE): Mission overview, *Geophys. Res. Lett*., **32**, L15S01, doi: 10.1029/2005GL022386.

Bozem, H., Fischer, H., Gurk, C., Schiller, C. L., Parchatka, U., Koenigstedt, R., Stickler, A., Martinez, M., Harder, H., Kubistin, D., Williams, J., Eerdekens, G., and Lelieveld, J. (2014), Influence of corona discharge on the ozone budget in the tropical free troposphere: a case study of deep convection during GABRIEL, *Atmos. Chem. Phys.*, **14**, 8917-8931, doi:10.5194/acp-14-8917-2014, 2014.

Brewer, A. W. (1949), Evidence for a world circulation provided by the measurements of

helium and water vapor distribution in the stratosphere, *Q. J. Roy. Meteorol. Soc.*, **75**, 351-363, doi: 10.1002/qj.49707532603.

Carminati, F., P. Ricaud, J. P., Pommereau, E., Riviere, S., Khaykin, J. L., Attie, and J., Warner (2014), Impact of tropical land convection on the water vapour budget in the tropical tropopause layer, *Atmos. Chem. Phys.*, **14**, 6195-6211, doi: 10.5194/acp-14-6195-2014.

Dee, D. P., et al. (2011), The ERA-Interim reanalysis: configuration and performance of the data assimilation system, *Q. J. Roy. Meteorol. Soc.*, **137**, 553–597, doi:10.1002/qj.828.

Dessler, A. E., and S. C. Sherwood (2003), A model of HDO in the tropical tropopause layer, *Atmos. Chem. Phys*., **3**, 2173-2181, doi: 10.5194/ acp-3-2173-2003.

Dessler, A. E., T. F. Hanisco, and S. Fueglistaler (2007), Effects of convective ice lofting on H_2O and HDO in the tropical tropopause layer, *J. Geophys. Res.*, **112**, D18309, doi: 10.10-29/2007JD008609.

Dessler, A. E. (2013), Observations of Climate Feedbacks over 2000-10 and Comparisons to Climate Models, *J. Climate*, **26**, 333-342, doi: 10.1175/JCLI-D-11-00640.1.

Dickerson, R. R., et al. (1987), Thunderstorms: An important mechanism in the transport of air pollutants, *Science*, **235**(4787), 460-465, doi: 1126/science.235.4787.460.

Draxler, R. R., and G. D. Hess (1998), An overview of the HYSPLIT_4 modelling system of trajectories, dispersion, and deposition, *Aust. Meteor. Mag*., **47**, 295-308.

Flury, T., D. L. Wu, and W. G. Read (2012), Correlation among cirrus ice content, water vapor and temperature in the TTL as observed by CALIPSO and Aura/MLS, *Atmos. Chem.*

Phys., **12**, 683-691, doi: 10.5194/acp-12-683-2012.

Forster, P. M. de F., and K. P. Shine (1997), Radiative forcing and temperature trends from stratospheric ozone changes, *J. Geophys. Res*., **102**, 10841–10855. doi: 10.10-29/1999GL0-10487.

Frey, W., et al. (2015), The impact of overshooting deep convection on local transport and mixing in the tropical upper troposphere/lower stratosphere (UTLS), *Atmos. Chems. Phys. Discuss*, **15**, 1041-1091.

Fu, R, Y. L. Hu, J. S. Wright, J. H. Jiang, R. E. Dickson, M. X. Chen, M. Filipiak, W. G. Read, J. W. Waters, and D. L. Wu (2006), Short circuit of water vapor and polluted air to the global stratosphere by convective transport over the Tibetan Plateau, *PNAS*, **103**(15), 5664-5669, doi: 10.1073/pnas. 0601584103.

Fueglistaler, S., A. Dessler, T. Dunkerton, I. Folkins, Q. Fu, and P. Mote (2009), Tropical tropopause layer, *Rev. Geophys.*, **47**, 1004, doi: 10.1029/2008RG00267.

Fueglistaler, S., Y. S. Liu, T. J. Flannaghan, F. Ploeger, and P. H. Haynes (2014), Departure from Clausius-Clapeyron scaling of water entering the stratosphere in response to changes in tropical upwelling, *J. Geophys. Res.*, **119**, 1962-1972, doi: 10.1002/2013JD020772.

Gettelman, A., P. Hoor, L. L. Pan, W. J. Randel, M. L. Hegglin, and T. Birner (2011), The extratropical upper troposphere and lower stratosphere, *Rev. Geophys.*, **49**, RG3003, doi: 10.1029/2011RG000355.

Hanisco, T. F., et al. (2007), Observations of deep convective influence on stratosphere water vapor and its isotopic composition, *Geophys. Res. Lett.*, **34**, L04814, doi: 10.1029/2006GL-

027899.

Hartmann, D. L., A. M. G. Klein Tank, M. Rusticucci, L. V. Alexander, S. Brönnimann, Y. Charabi, F. J. Dentener, E. J. Dlugokencky, D. R. Easterling, A. Kaplan, B. J. Soden, P. W. Thorne, M. Wild, and P. M. Zhai (2013), Observations: Atmosphere and Surface In: *Climate Change 2013: The Physical Science Basis. Contribution of Working Group I to the Fifth Assessment Report of the Intergovernmental Panel on Climate Change* [Stocker, T. F., D. Qin, G.-K. Plattner, M. Tignor, S. K. Allen, J. Boschung, A. Nauels, Y. Xia, V. Bex, and P. M. Midgley, (eds)], Cambridge University Press, Cambridge, United Kingdom and New York, NY, USA, pp. 159-254, doi: 10.1017/CBO9781107415324.008.

Hegglin, M. I., et al. (2013), SPARC Data Initiative: Comparison of water vapor Climatologies from international satellite limb sounders, *J. Geophys. Res. Atmos.*, **118**, 11824–11846, doi:10.1002/jgrd.50752.

Hegglin, M. I., D. A. Plummer, T. G. Shepherd, J. F. Scinocca, J. Anderson, L. Froidevaux, B. Funke, D. Hurst, A. Rozanov, J. Urban, T. von Clarmann, K. A. Walker, H. J. Wang, S. Tegtmeier, and K. Weigel (2014), Vertical structure of stratospheric water vapour trends derived from merged satellite data, *Nature Geosci*, **7**, 768-776, doi: 10.1038/ngeo2236.

Hingane, L. S. (1989), Effect of increasing CO_2 on the stratospheric level of CO and O_3, *Adv. Atmos. Sci.*, **6**, 390-392, doi: 10.1007/BF02661544.

Holton, J. R., and A. Gettelman (2001), Horizontal transport and the dehydration of the

stratosphere, Geophys. Res. Lett., 28, 2799-2802, doi: 10.1029/2001GL013148.

Huang, Y. (2013), On the longwave climate feedback, *J. Climate*, **26**, 7603-7610, doi: 10.1175/JCLI-D-13-00025.1.

Iwasaki, S., T., Shibata, H., Okamoto, H., Ishimoto, and H., Kubota (2012), Mixtures of stratospheric and overshooting air measured using A-Train sensors, *J. Geophys. Res. Atmos.*, **117**, D12207, doi: 10.1029/2011JD017402.

Jiang, J. H., et al. (2012), Evaluation of Cloud and Water Vapor Simulations in CMIP5 Climate Models Using NASA A-Train Satellite Observations, *J. Geophys. Res.*, **117**, D1410, 24 PP, doi: 10.1029/2011JD017237.

Jiang, J. H., et al. (2010), Five-year (2004-2009) Observations of Upper Tropospheric Water Vapor and Cloud Ice from MLS and Comparisons with GEOS-5 analyses, *J. Geophys. Res.*, **115**, D15103, doi: 10.1029/2009JD013256.

Kalnay, E., et al. (2006), The NCEP/NCAR 40-year reanalysis project, *Bull. Amer. Meteor. Soc.*, **77**, 437-470, doi: 10.1175/1520-0477(1996)077<0437:TNYRP>2.0.CO;2.

Kley, D., et al. (1996), Observations of near-zero ozone concentrations over the convective Pacific: Effects on air chemistry, *Science*, **274**, 230 – 233, doi:10.1126/science.274.5285.-230.

Kubar, T. L., D. L. Hartman, and R. Wood (2007), Radiative and convective driving of tropical high clouds, J. Climate, 20, 5510-5526.

Laing, A. G., and J. M. Fritsch (2007), The global population of mesoscale convective

complexes, Q. J. R. Meteorol. Soc., 123, 389-405, doi: 10.1002/qj.49712353807.

Livesey, N. J., W. Van Snyder, W. G. Read, and P. A. Wagner (2006), Retrieval algorithms for the EOS Microwave Limb Sounder (MLS), *IEEE Trans. Geosci. Remote Sens.*, **44**, 1144-1155, doi: 10.1002/jgrd.50800.

Livesey, N. J., et al. (2008), Validation of Aura Microwave Limb Sounder O_3 and CO observations in the upper troposphere and lower stratosphere, *J. Geophys. Res.*, **113**, D15S02, doi: 10.1029/2007JD008805.

Livesey, N. J., et al. (2011), EOS MLS Version 3.3 Level 2 data quality and description document version 3.3x-1.0, JPL D-33509, Jet Propul. Lab., Pasadena, Calif.

Livesey, N. J., et al. (2013), Interrelated variations of O_3, CO and deep convection in the tropical/subtropical upper troposphere observed by the Aura Microwave Limb Sounder (MLS) during 2004-2011, *Atmos. Chem. Phys.*, **13**, 579-598.

Machado, L. A. T., and W. B. Rossow (1993), Structure characteristics and radiative properties of tropical cloud clusters, *M. Weather Rev.*, **121**, 3234-3260, doi: 10.1175/1520-0493(1993)-121<3234: SCARPO> 2.0.CO;2.

Machado, L. A. T., W. B. Rossow, R. L. Guedes, and A. W. Walker (1998), Life cycle variations of mesoscale convective systems over the Americas, *Mon. Wea. Rev.*, **126**, 1630-1654, doi: 10.1175/1520-0493(1998)1262.0.CO;2.

Newman, P. A., J. C. Wilson, M. N. Ross, C. A. Brock, P. J. Sheridan, M. R. Schoeberl, L. R. Lait, T. P. Bui, M. Loewenstein, and J. R. Podolske (2001), Chance encounter with a stratospheric kerosene rocket plume from Russia over California, *J. Geophys. Res. Lett.*, **28**, 959-

962.

Pickering K. E., A. M. Thompson, W.-K. Tao, and T. L. Kucsera (1993), Upper Tropospheric Ozone Production Following Mesoscale Convection during STEP/EMEX, *J. Geophys. Res.*, **98**, 8737-8749.

Poulida, O., R. R., Dickerson, and A. Heymsfield (1996), Stratosphere-troposphere exchange in a midlatitude mesoscale convective complex: 1. Observations, *J. Geophys. Res.*, **101**, 6823-6836, doi: 10.1029/95JD03523.

Read, W. G., et al. (2007), Aura Microwave Limb Sounder upper tropospheric and lower stratospheric H_2O and relative humidity with respect to ice validation, J. Geophys. Res., 112, D24S35, doi: 10.1029/2007JD008752.

Randel, W. J., E. Moyer, M. Park, E. Jensen, P. Bernath, K. Walker, and C. Boone (2012), Global variations of HDO and HDO/H_2O ratios in the upper troposphere and lower stratosphere derived from ACE-FTS satellite measurements, *J.Geophys. Res.*, **117**, D06303, doi: 10.1029/2011JD016632.

Ray, E. A., and K. H. Rosenlof (2007), Hydration of the upper troposphere by tropical cyclones, *J. Geophys. Res.*, **112**, D12311, doi: 10.1029/2006JD008009.

Rossow, W. B., A. W. Walker, D. Beuschel, and M. Roiter (1996), International Satellite Cloud Climatology Project (ISCCP) Description of New Cloud Datasets. WMO/TD – No. 737, World Climate Research Programme (ICSU and WMO), Geneva, February 1996, pp. 115.

Sahu, L. K., and S., Lal (2006), Changes in surface ozone levels due to convective down-drafts over the Bay of Bengal, *Geophys. Res. Lett.,* **33**, L10807, doi: 10.1029/2006GL-025994.

Schwartz, M. J., W. G. Read, M. L. Santee, N. J. Livesey, L. Froidevaux, A. Lambert, and G. L. Manney (2013), Convectively injected water vapor in the North American summer lowermost stratosphere, *Geophys. Res. Lett*., **40**, 2316-2321, doi: 10.1002/grl.50421.

Solomon, S., D. W. J. Thompson, R. W. Portmann, S. J. Oltmans, and A. M. Thompson (2005), On the distribution and variability of ozone in the tropical upper troposphere: Implications for tropical deep convection and chemical-dynamical coupling, *Geophys. Res. Lett.*, **32**, L23813, doi: 10.1029/2005GL024323.

Solomon, S., K. Rosenlof, R. Portmann, J. Daniel, S. Davis, T. Sanford, and G.-K Plattner (2010), Contributions of Stratospheric Water Vapor to Decadal Changes in the Rate of Clobal Warming, *Science*, **327**, 1219, doi: 10.1126/science.1182488.

Rodriguez, J. M., K. W. Ko, Malcolm, and D. S., Nien (2012), *Geohys. Res. Lett.*, **13**, 499-502, doi: 10.1029/GL013i006p00499.

Strong, M., Z. D. Sharp, and D. S. Gutzler (2007), Diagnosing moisture transport using D/H ratios of water vapor, *J. Geophys. Res. Lett..*, **34**, L03404, doi: 10.1029/2006GL028307.

Takahashi, H., and Z. J. Luo (2014), Characterizing tropical overshooting deep convection from joint analysis of CloudSat and geostationary satellite observations, *J. Geophys. Res. Atmos.*, **119**, 112-121, doi: 10.1002/2013JD020972.

Vogel, B., W., Feng, M., Streibel, and R., Muller (2006), The potential impact of ClO_X

radical complexes on polar stratospheric ozone loss processes, *Atmos. Chem. Phys.*, **6**, 3099-3114.

Wang, T., W. J. Randel, A. E. Dessler, M. R. Schoeberl, and D. E. Kinnison (2014), Trajectory model simulations of ozone (O_3) and carbon monoxide (CO) in the lower stratosphere, *Atmos. Chem. Phys.*, **14**, 7135-7147, doi: 10.5194/acp-14-7135-2014.

Wardle, D. (1997), Ozone science: A Canadian perspective on the changing ozone layer, Ottawa, Canada: Environment Canada.

Weinstock, E. M., et al. (2009), Validation of the Harvard Lyman-α in situ water vapor instrument: Implications for the mechanisms that control stratospheric water vapor, *J. Geophys. Res.*, **114**, D23301, doi: 10.1029/2009JD012427.

World Meteorological Organization (WMO) (1957), Meteorology A Three-Dimensional Science: Second Session of the Commission for Aerology, WMO Bulletin IV(4), WMO, Geneva, 134-138.

Wright, J. S., R. Fu, S. Fueglistaler, Y. S. Liu, and Y. Zhang (2011), The influence of summertime convection over Southeast Asia on water vapor in the tropical stratosphere, *J. Geophys. Res.*, **116**, D12302, doi: 10.1029/2010JD015416.

Yuan, T. and Z. Li (2009), General macro- and microphysical properties of deep convective clouds as observed by modis, J. Climate, 23, 3457-3473.

Zipser, E. J., D. J. Cecil, C. Liu, S. W. Nesbitt, and D. P. Yorty (2006), Where are the most intense thunderstorms on earth?, Bull. Amer. Meteor. Soc., 87, 1057-1071.